Chemical Engineering Journal 509 (2025) 161494

Contents lists available at ScienceDirect

Chemical Engineering Journal

journal homepage: www.elsevier.com/locate/cej

Energy-dense sustainable aviation fuel-range hydrocarbons from cyclohexanone as a biomass-derived feedstock via sequential catalytic aldol condensation and hydrodeoxygenation

Abarasi Hart, Jude A. Onwudili *, Eyup Yildirir, Seyed E. Hashemnezhad

Energy and Bioproducts Research Institute, College of Engineering and Physical Sciences, Aston University, Aston Triangle, Birmingham B4 7ET, United Kingdom

ARTICLE INFO

Keywords:
Lignin-derived bio-oil
Cyclohexanone
Aldol condensation
Hydrogenation
Sustainable Aviation fuel-range hydrocarbons
Niobium phosphate-based catalysts

ABSTRACT

Climate change is the main driver for sustainable aviation fuels production as a means of decarbonising/defossilising the sector. In this work, several catalysts have been screened to produce aviation fuel (C_6-C_{16}) component hydrocarbons from cyclohexanone, a model compound of lignin-derived bio-oils. Using a two-stage two-pot approach, up to 99 % cyclohexanone conversion was achieved in the presence of hydrogen gas. In the first stage, catalytic activities of $NbOPO_4$, Al_2O_3, SiO_2, and ZrO_2-SiO_2 to promote aldol condensation were tested at 160 °C for 3 h. The $NbOPO_4$ exhibited the highest selectivity towards C-C coupling adducts with mainly C_{12} to C_{18}. In the second stage, 30 wt% Ni catalysts on three different supports and 5 wt% Pd/Al_2O_3 were used to catalyse the hydrogenation of the first-stage adducts at 300 °C for 3 h. The 30 wt%Ni/$NbOPO_4$ was most effective, promoting the formation of bi-cycloalkanes, alkyl aromatic, and partially hydrogenated polyaromatic hydrocarbons. In comparison, a one-pot two-step approach was tested by sequentially reacting cyclohexanone with hydrogen gas over the two temperatures for 3 h each, using 30 wt%Ni/$NbOPO_4$ as catalyst. Reacting cyclohexanone with 10 wt% bio-oil samples led to significantly reduced first stage conversion, and enhanced yields of single C-C coupled oxygenates and almost no hydrocarbons in the second stage. Overall, combination of catalysts and hydrogen gas over staged reactions has effectively converted pure cyclohexanone into naphthene-rich liquid hydrocarbons and cyclohexanone/bio-oil mixed feedstocks into their oxygenated precursors. These results support potential targeted production of bio-derived sustainable alternative fuels for the defossilisation of aviation industry.

1. Introduction

While the road transportation sector has made significant strides towards NetZero with electric powered vehicles, the aviation and marine transportation sectors are still trailing behind in the deployment of sustainable alternatives for petroleum-based fuels. Globally, aviation fuels account for about 12 % of the liquid transportation fuels utilised today [1], and as a result, approximately 13 % of greenhouse gas (GHG) emissions from transportation can be ascribed to commercial aviation [2]. Thus, one of the major transportation sectors requiring decarbonisation is the aviation industry. However, decarbonising the aviation industry through electrification, especially for long haul flights, seems a remote reality at present. It has therefore become imperative to take advantage of novel synthetic methods to produce aviation fuels from sustainable and low-carbon lignocellulosic biomass [3,4]. Catalytic conversion of lignocellulosic biomass-derived feedstocks and molecules into fuels and chemicals is of significant relevance and attractive in response to climate change awareness caused by over-dependence on fossil resources. Hence, bio-oils derived from pyrolysis of lignocellulosic biomass can be upgraded into liquid hydrocarbons with carbon number in the range of gasoline, aviation fuel (kerosene) and diesel [5,6]. In addition, producing drop-in liquid transportation fuels and organic chemicals from biomass will also facilitate sustainability and promote sustainable development across various regions of the world with abundant biomass resources.

Conventional aviation fuels are composed of hydrocarbons, which are mainly *n*-alkanes, branched alkanes, cycloalkanes, and alkyl aromatics [7]. Among these hydrocarbons, the cycloalkanes, bi-cycloalkanes, and aromatic components are known to improve the volumetric heating values and thermal stability of aviation fuels due to

* Corresponding author.
E-mail address: j.onwudili@aston.ac.uk (J.A. Onwudili).

https://doi.org/10.1016/j.cej.2025.161494
Received 1 August 2024; Received in revised form 18 January 2025; Accepted 10 March 2025
Available online 11 March 2025

their high densities [1,2,7]. These high energy–density hydrocarbons maximize aircraft range and low freezing point to prevent crystalline wax formation during flight, making them the two most important requirements for aviation fuels [7,8]. Therefore, from a synthesis point of view, it is vital to concentrate efforts at producing those valuable components of aviation fuels from biomass, where possible. This will both support efficient utilisation of biomass resources and the knock-on effect of reducing overall carbon emissions due to cleaner combustion and efficiency gains in aircraft engine performance.

Since pyrolysis bio-oils and other biomass-derived platform molecules have few carbon numbers (C_2-C_8), the process of producing sustainable aviation fuels from bio-oils should involve controlled C–C coupling reactions. Organic chemical reactions leading to C-C coupling can be achieved through aldol condensation, ketonisation, alkylation and other reactions based on certain functional groups. After successful C-C coupling, the resulting products with fuel relevant carbon chains can be subsequently converted to hydrocarbons using hydrodeoxygenation (HDO) techniques [9]. Relevant HDO techniques include those that retain all or most of the carbon atoms in the C-C coupled products, while removing oxygen atoms.

Aldol condensation is a well-known C-C chain elongation reaction of carbonyl compounds (ketones and aldehydes) [10,11]. These compounds can account for up to 30 % relative content of fast pyrolysis and of this, more than 22 % can be ketones [12]. Hence, ketones represent a large proportion of fast pyrolysis bio-oils and studying their catalytic reactions during bio-oil upgrading to fuel-relevant long-chain hydrocarbons has become very important to improve yields. During catalytic upgrading of bio-oils or its constituent compounds, the yields of liquid products are determined by the reaction conditions, nature of feedstock and the choice of catalyst. For example, one-pot aldol condensation and hydrodeoxygenation of biomass-derived furfural and acetone to produce biodiesel hydrocarbon range has been reported over Pt/Mg–Zr mixed oxides and Pt/AC + MgZr/HSAG500 catalysts [13]. They found that the selectivity towards *n*-alkanes was higher than 50 % at temperature 220 °C, pressure 45 bar after 24 h reaction time.

Among ketones found in bio-oils, many researchers [4,11,14] have used cyclopentanone as a model ketone for conversion to aviation fuel range hydrocarbons, using different catalysts with some success. For instance, the conversion of cyclopentanone to fuel range hydrocarbons using one-pot catalytic systems has been reported [4]. Wang et al. [4] synthesised 1-(3-Cyclopentyl)cyclopentyl-2-cyclopentylcyclopentane from cyclopentanone produced from hemicellulose. The researchers used Raney metal and alkali hydroxides for self-aldol condensation stages, and Ni-SiO_2 catalyst for the solvent-free hydrodeoxygenation step over three stages [4]. The conversion achieved was 88.5 % at temperature 260 °C, hydrogen pressure 60 bar, and catalyst loading 1.8 g for flow reactor system. In another one-pot approach, Li et al. [11] studied the aldol condensation of cyclopentanone over Ni/Mg-Al-O/AC bifunctional catalysts at low-temperature condensation (170 °C) for 6 h, followed by high-temperature hydrogenation (260 °C) for 6 h, achieving a conversion of 94.7 % and hydrocarbon yield of 70 %, respectively [11]. Similarly, a one-pot aldol condensation of cyclopentanone followed by hydrogenation into aviation fuel range hydrocarbons with Mg-Al oxide catalyst resulted in 80.4 % yield of dimers and trimers due to its strong mild-basic sites at a temperature of 170 °C, catalyst 2.4 g, and cyclopentanone 8 mL. Loading 20 wt% Ni on Mg-Al-O/AC (activated carbon) catalyst provided appropriate active sites for hydrogenation resulting in 81.1 % yield of alkanes in the range of $C_{10} + C_{15}$ at 260 °C temperature, 30 bar hydrogen pressure, and 12 h reaction time [14]. In general, these studies show that the production of aviation fuel hydrocarbon range required long reaction times and could also be limited by low yields of aldol condensation products as well as competing side reactions. High yields of cyclohexanone have been reported directly from the hydrogenation of phenols, anisole, guaiacols, syringol, vanillin, and eugenol that compose lignin-derived bio-oils [5,15]. For example, researchers have shown that hydrogenation and hydrolysis of anisole can produce 96 % yield of cyclohexanone using bromide salt-modified Pd/C in H_2O/CH_2Cl_2 at 90 °C and hydrogen pressure 2 MPa [16]. In addition, it can be produced by selective hydrogenation of lignin-derived phenols over Pd-supported on carbon or alumina with selectivity of 99.9 % at 50 °C and 1 MPa [17]. Bakhtyari et al. [18] reported the use alumina-supported CoMo and NiMo catalysts at temperature 400 °C and pressure 15 bar (H_2), in a microactivity-reference fixed-bed catalytic reactor to study the catalytic hydrodeoxygenation (HDO) of cyclohexanone into liquid fuel-grade products. The authors reported a liquid product that composed mostly of C_6 compounds including cyclohexene, phenol, benzene, cyclohexanol, and cyclohexane [18]. The range of compounds must have been formed from a single cyclohexanone moiety, confirming that catalysts were unable to accomplish the desired C-C chain elongation during the HDO process.

In this present work, cyclohexanone has been reacted solvent-free with hydrogen gas in the presence of a selection of catalysts through self-aldol condensation and HDO to produce aviation fuel range of hydrocarbons. Two different approaches were investigated in attempt to improve the yields of final liquid products. In a two-pot approach, the self-condensation of cyclohexanone was studied using synthesised $NbOPO_4$ as catalyst. $NbOPO_4$ was selected as it has been reported to have excellent water-tolerant acid properties [19–22], with strong Brønsted and Lewis acid sites capable of catalysing C-C coupling creation during aldol condensation [20]. In addition, different nickel-supported catalysts including 30 wt% Ni/$NbOPO_4$, 30 wt% Ni/SiO_2, 30 wt%Ni/ZrO_2-SiO_2 and 5 wt% Pd/Al_2O_3, were screened for the hydrodeoxygenation (HDO) stage, using the recovered first-stage aldol condensation products. Literature has shown that significantly more transition metals loading, ranging from 10 − 60 wt% have been used to obtain HDO results comparable to 2–5 wt% loadings of noble metals like Pt and Pd during the conversion of pyrolysis bio-oils or to oxygenated model compounds [23,24]. For example, titania-supported Ni catalysts with Ni loading in the range of 10 to 60 wt% was applied to produce sustainable diesel through selective deoxygenation of natural triglyceride (sunflower oil), [25]. The results showed that the yield of diesel range n-alkanes increases with the Ni content of the catalyst up to 30 wt %, remaining almost unchanged at higher loadings. In comparison, a one-pot approach was tested by reacting cyclohexanone in the presence of $NbOPO_4$, 10 wt% Ni/$NbOPO_4$ and 30 wt% Ni/$NbOPO_4$ at low temperature for aldol condensation before increasing the temperature for HDO. The experimental design was planned to provide insights into the reaction mechanisms and processing conditions to produce high density aviation fuel hydrocarbons such as mono- and bi-cycloalkanes, alkyl cycloalkanes, and alkyl aromatics. The aim of this present work was to demonstrate the efficiency of low-cost non-noble niobium-based catalysts for the efficient solvent-free conversion of a cyclic ketone into high-density fuel range liquid hydrocarbons via a series of reactions. In addition, preliminary tests were carried out using 9:1 mass ratios of cyclohexanone and two types of pyrolysis bio-oils, to assess the influence of other components in bio-oil on the conversion of cyclohexanone via aldol condensation in the presence of 30 wt% Ni/$NbOPO_4$ catalyst using two-pot and one-pot systems, respectively. The work has the potential to provide the basis for the future process development of a viable chemical process to produce sustainable liquid hydrocarbons from biomass, particularly within the range of aviation fuels.

2. Experimental

2.1. Materials

Liquid feedstocks included cyclohexanone feedstock (99+% purity, Fisher Scientific, Leicester, UK), and two bio-oil samples (Bio-oil A and Bio-oil B) produced in-house at the Energy and Bioproducts Research Institute (EBRI), Aston University. Bio-oil A was produced from a mixed biomass feedstock while Bio-oil B was produced from rice straw. All the materials for catalyst preparation including, sodium silicate

nanohydrate ($Na_2SiO_3{\cdot}9H_2O$), zirconyl chloride octahydrate ($ZrOCl_2{\cdot}8H_2O$), ammonia hydroxide, diammonium hydrogen phosphate, niobium(v) oxalate hydrate, hydrochloric acid, phosphoric acid, cetyltrimethyl ammonium bromide (CTAB), and nickel(II) nitrate hexahydrate were all purchased from Fisher Scientific, Leicester, UK. Commercial 5 wt% Pd/Al_2O_3 catalyst was purchased from Catal International Limited, Sheffield, UK.

2.2. Catalyst preparation and characterisation

The following catalysts/support materials were prepared by precipitation and co-precipitation: SiO_2, ZrO_2, SiO_2-ZrO_2. A total of 40 g of the precursors ($ZrOCl_2{\cdot}8H_2O$ and $Na_2SiO_3{\cdot}9H_2O$) was dissolved in 400 mL of distilled water and stirred vigorously at room temperature. Ammonia hydroxide solution was added dropwise to the solution of $ZrOCl_2{\cdot}8H_2O$ until the pH is in the range of 9 – 10, while hydrochloric acid was added to $Na_2SiO_3{\cdot}9H_2O$ solution to achieve a pH range of 8 – 9. The suspension was mixed vigorously at 60 °C for 6 h and aged for 24 h. The precipitate obtained in each case was filtered, dried at 80 °C for 4 h, and calcined at 500 °C for 4 h.

Preparation of $NbOPO_4$ was carried out according to the method reported by Zhang et al. [23]. First, 28.055 g of niobium(v) oxalate hydrate ($C10H_2Nb_2O_{21}$) was dissolved in 100 ml of distilled water. Then approximately, 6.6 g (0.01 mol) of diammonium hydrogen phosphate ($(NH_4)_2HPO_4$) was also dissolved in a separate 100 ml of distilled water. Both solutions were vigorously mixed in 500 ml beaker using a magnetic stirrer, and the pH of the mixture adjusted to 2 using phosphoric acid. Furthermore, a solution of CTAB was prepared by dissolving 5.0 g of CTAB in 75 mL of distilled water and added to the earlier mixture, while maintaining the pH of the final solution at 2 with more phosphoric acid. Subsequently, the final mixture was stirred with the aid of magnetic stirrer for 60 min at 35 °C, to produce a white gel. Ageing of the white gel was achieved in a Teflon-lined autoclave at 160 °C for 24 h, leading to the precipitation of $NbOPO_4$ under hydrothermal conditions. Thereafter, the NbOPO4 was recovered by filtration, washed severally with distilled water until the wash water reached a PH of 7. Finally, the solid was dried at 100 °C and any organic residuals in the NbOPO4 was removed by calcination in air at 500 °C for 4 h.

Four nickel catalysts on different supports including 10 wt% Ni/$NbOPO_4$, 30 wt% Ni/$NbOPO_4$, 30 wt% Ni/SiO_2, and 30 wt% Ni/ZrO_2-SiO_2 were prepared using wet impregnation method. In this case, an appropriate amount of nickel precursor $Ni(NO_3)_2{\cdot}6H_2O$ was dissolved in 5 mL distilled water for 30 min using a magnetic stirrer. Thereafter, the required amount of the support material (2 g) was added and stirred for 1 h at ambient temperature. The resulting slurry was dried at 100 °C overnight and calcined at 500 °C for 4 h to produce the different catalyst catalysts.

Nitrogen physisorption technique was applied to determine the surface areas, pore volumes, and pore size distributions of the prepared catalysts using the Quantachrome Instruments NOVA 4200. Whereas X-ray diffraction (XRD) Bruker D8 Advance A25 was used to analyse the bulk crystal structure and phase composition of the catalysts. The different types of acid sites (Brønsted and Lewis acidic sites), number, and their relative strength on the surface of catalysts were determined using a pyridine Fourier-transform infrared (pyridine-FTIR) spectroscopy technique. The adsorption of pyridine was tracked by infrared spectroscopy, which was recorded using a Nicolet iS50 FTIR Spectrometer, Thermo Scientific at a resolution of 4 cm^{-1}. This method of determining and quantifying acid sites has been reported extensively in the literature [23–25]. Consequently, Inductively Coupled Plasma Optical Emission Spectroscopy (ICP-OES) technique was used to quantify the Ni metal loading on the catalysts. A small quantity of each sample was digested in 20 mL aqua regia (HNO_3:HCl = 30:70 v/v) for 24 h before being analysed with iCAP 7000 series ICP-OES Spectrometer-elemental analyser (Thermo Fisher Scientific).

2.3. Catalytic experiments with cyclohexanone

The experimental conditions of reaction temperature (160 °C and 300 °C and 10 bar initial hydrogen pressure) and reaction times (1 h – 3 h) used in this work largely followed the successful novel solvent-assisted catalytic HDO upgrading of bio-oil produced via fast pyrolysis of lignocellulosic biomass published in the literature [5].

2.3.1. Two-stage two-pot aldol condensation and hydrogenation experiment

In the two-pot approach, both the aldol condensation of the cyclohexanone and hydrodeoxygenation (HDO) of the condensed products were carried out using a 100 ml Parr batch reactor (Parr Instrument Company, Moline, IL, USA) over two stages. In the first stage, a solvent-free aldol condensation was carried out by reacting 10 g of cyclohexanone in the presence of 0.5 g NbOPO4 at 160 °C temperature for 3 h reaction time using 10 bar initial hydrogen gas pressure. The $NbOPO_4$ catalyst was suspended by glass wool inside the reactor, above the level of the cyclohexanone liquid to facilitate vapour-catalyst contact and post-reaction recovery of products. A preliminary experiment was conducted to contrast supporting the catalyst on glass wool on top of the feedstock and directly mixing the catalyst with cyclohexanone in the reactor. In 3 h reaction time at 160 °C, 5 bar initial nitrogen pressure, and 0.2 g catalyst loading, the glass wool suspended catalyst achieved 76.7 % conversion, whereas the catalyst mixed directly with cyclohexanone in the reactor produced 57.8 %. Better interactions between the reactants and catalyst are likely responsible for the greater conversion that was attained with the glass wool supported catalyst. However, with and without glass wool (i.e., without catalyst), about 14 % cyclohexanone conversion was achieved at the same experimental conditions. Subsequently, HDO of the adduct from Stage 1 (≈ 8 g) was performed using the same reactor, with 0.5 g of each of the synthesised supported Ni catalysts and 5 wt% Pd/Al_2O_3. The second stage experiment was carried out at 300 °C temperature using 10 bar initial hydrogen pressure for reaction times of 3 – 6 h. Fig. 1**a** shows the experimental protocols for the two-pot approach. At the end of the experiments, the reactor was rapidly cooled to ambient temperature using a laboratory fan prior to product recovery and analyses.

A major focus of this work was to reduce the hydrogen consumption during HDO. This was proved in a previous work [5,26], where the combination 10 bar hydrogen with solvent was effective for HDO. Moreover, the results from this present work have shown that 10 bar hydrogen was sufficient for the two-stage process, and we have presented our results based on these parameters.

2.4. One-pot two-step sequential aldol condensation and hydrogenation experiment

In the one-pot approach, the aldol condensation of cyclohexanone followed by the HDO was carried out sequentially without opening the reactor or changing the gas environment. The aldol condensation of cyclohexanone was performed at 160 °C, using 0.5 g of catalyst, 10 g cyclohexanone, 10 bar initial hydrogen pressure, and 3 h reaction time. Three niobium phosphate-based catalysts ($NbOPO_4$, 10 wt% Ni/$NbOPO_4$ and 30 wt% Ni/$NbOPO_4$) were used in this case. At the end of 3 h at 160 °C, the temperature was increased to 300 °C for the HDO process for another 3 h reaction time (Fig. 1b). Identical analytical protocols described for the two-pot approach were used to determine product yields.

2.5. Product analysis

Once the reactor had cooled to ambient temperature, the produced gas was collected using gas 1 L Tedlar gas bag, where applicable. Notably, no significant gas products were obtained after the first stage of the two-pot system and were not analysed. The reactor was then opened to recover the liquid product, which was further separated from solids

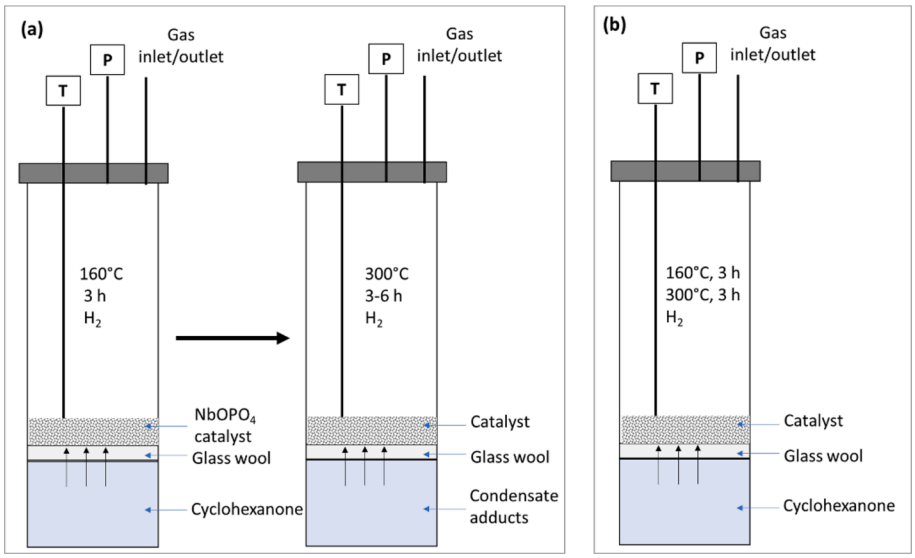

Fig. 1. Schematic illustration of (a) two-pot and (b) one-pot reaction systems.

by filtration. The spent catalyst was also recovered, dried and weighed.

Considerable amounts of gas products were obtained the second stage of the two-pot system and the one-pot sequential system. These gas products were compositionally analysed by injecting 0.6 cm^3 into a gas chromatograph (GC-2014, Shimadzu Gas Chromatograph). A flame ionization detector (FID) and a thermal conductivity detector (TCD) were used to quantify $C_1 - C_4$ hydrocarbon gases and permanent gases (such as N_2, H_2, CO, and CO_2, respectively. The compositions and distribution of organic compounds in the liquid-like (first stage) and liquid products (second stage) were determine using a gas chromatography–mass spectrometer GC–MS (GCMS-QP2010 SE, Shimadzu). The conversion of cyclohexanone was calculated using Equation (1), while the selectivity towards certain hydrocarbons was calculated by Equation (2). The coke content of the spent catalyst following the reaction was estimated based on thermogravimetric analyser (TGA) technique (TGA/DSC 2 STAR^e System, Mettler-Toledo). The temperature programme was ramped from 40 to 900 °C, and the furnace was heated at a rate of 10 °C/min followed by 15 min isothermal condition at 900 °C with air flowing at 30 cm^3/min. The conversion of cyclohexanone is calculated using Equation (1), while the selectivity of product is calculated using Equation (2).

$$Conversion[\%] = \frac{Moles_{CYi} - Moles_{CYf}}{Moles_{CYi}} \times 100 \quad (1)$$

$Moles_{CYi}$ = mole of cyclohexanone fed into the reactor

$Moles_{CYf}$ = mole of cyclohexanone recovered after reaction

$$Selectivity[\%] = \frac{\text{Peak Area of component i}}{\text{Total Peak Area of all Components identified}} \times 100 \quad (2)$$

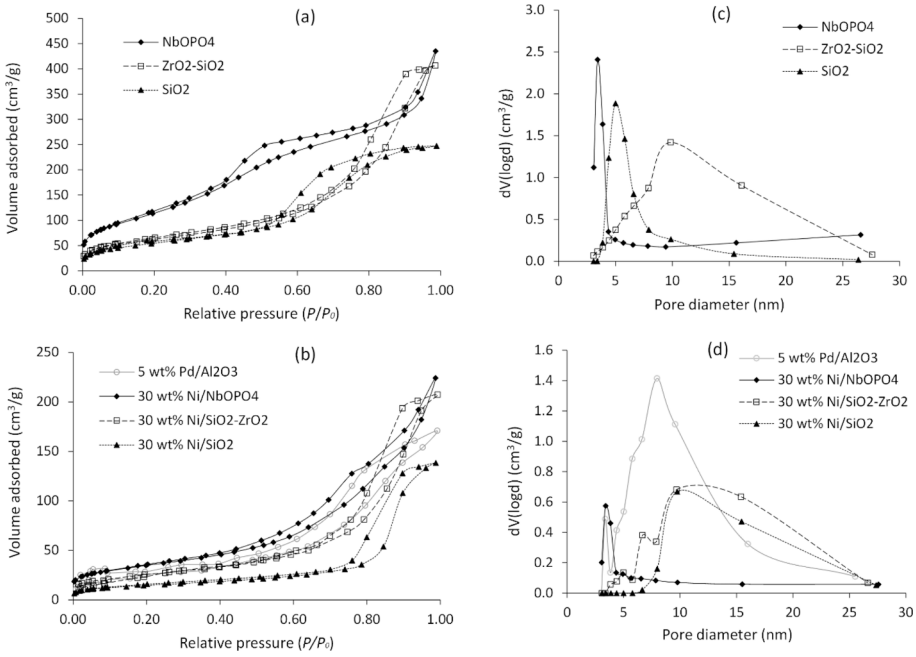

Fig. 2. Catalyst textural characteristics: (a) N_2 adsorption–desorption isotherm for synthesised supports, (b) isotherms for supported metal catalysts, (c) pore size distribution for synthesized supports, and (d) pore size distribution for supported metal catalysts.

3. Results and discussion

3.1. Catalyst characterisation

3.1.1. Textural characteristics

The catalytic performance of the catalysts depends on the physico-chemical properties. The specific surface area and porosity are among the critical properties that determine catalytic activity and selectivity. Fig. 2 shows the nitrogen adsorption–desorption isotherms and pore size distributions of the synthesised support materials and metal-supported catalysts. The isotherm hysteresis loop indicate that they were Type IV (Fig. 2**a,b**), consistent with the presence of mesoporous structures. The pore volumes of the catalyst support materials were dominated by mesopores of sizes between 2 nm and 50 nm. The pore size range were as follows: $NbOPO_4$ (3 nm to 5.7 nm), SiO_2 (3.8 nm to 8 nm), and ZrO_2-SiO_2 (6 nm to 16 nm). It is evident from Fig. 2**c** that ZrO_2-SiO_2 has larger pore diameters than SiO_2, while $NbOPO_4$ has narrower mesopores when compared to the other materials. Brunauer–Emmett–Teller (BET) and Barrett–Joyner–Halenda (BJH) equations were used to determine the specific surface area and pore size distribution of the catalyst support materials. The pore size distribution and pore volume were obtained from the isotherm desorption branch using the BJH model based on multipoint method. The relative pressure values were used to determine pore diameters using Kelvin equation, and the BJH model used to compute the pore size distribution of the markedly mesoporous material. The results are summarised in Table 1. Among the synthesised supports, $NbOPO_4$ possessed the largest surface area followed by ZrO_2-SiO_2, and then SiO_2. However, the impregnation of NiO nanoparticles onto the support materials narrowed the pore sizes which is evident in the shift of the hysteresis loop towards high relative pressure (Fig. 2**b**). The impregnated Ni metal mostly plugged pore diameter less than or equal to 7 nm, while narrowing pore sizes greater than 7 nm (Fig. 2**d**). This resulted in significant decrease in the surface areas and pore volumes of the respective catalysts (Table 1). The drop in surface area as a result of incorporating NiO nanoparticles are as follows: 58.52 % (30 wt % Ni/ ZrO_2-SiO_2), 69.68 % (30 wt% Ni/ $NbOPO_4$), and 72.94 % (30 wt% Ni/SiO_2). NiO nanoparticles formed from the calcination of impregnated nickel (II) nitrate solution have been reported in the literature to produce crystallites of different sizes, some of which could be smaller or larger than the pore size of the catalyst support [27]. Hence, NiO particles smaller than the pore sizes of the support may be imbibed into these pores, while larger particles would remain outside the pores. While the location of the NiO particles relative to the porous support was not the subject of this present work, the metal loading ascribed to the presence of NiO crystallites was confirmed by XRD (**Section 3.1.2**).

3.1.2. X-ray diffraction (XRD) pattern

The XRD patterns of the support materials and the synthesised catalysts are shown in Fig. 3. The synthesised SiO_2 and ZrO_2-SiO_2 materials showed one broad peak at about 2θ equals 22.5°, indicating that the prepared silica and zirconia-silica supports are known to be amorphous. The broad peak also indicates that the silica particle size is nanosized. Likewise, the XRD patterns of $NbOPO_4$ materials and 10 wt% Ni/$NbOPO_4$ show two broad peaks at $2\theta = 25°$ and 53°, demonstrating that the material was amorphous. The observation on 10 wt% Ni/$NbOPO_4$ could be attributed to low metal loading and, consequently, NiO nanoparticles became well dispersed on the support material. However, increasing Ni loading to 30 wt% on SiO_2, ZrO_2-SiO_2, and $NbOPO_4$ resulted in XRD patterns with peaks at $2\theta = 37°$, 43°, 63°, 75°, and 79°. These peak positions correspond to the characteristic peaks of NiO, which indicates the following crystal planes (111), (200), (220), (311), and (222) [28,29]. They are indexed to face centred cubic (FCC) NiO crystalline structure [28]. Since no other distinctive peaks other than the FCC NiO phase can be found on the XRD pattern of Ni-supported on silica, niobium phosphate, and silica-zirconia, the catalysts are considered a single-phase with no impurities. The decomposition of impregnated nickel (ii) nitrate during calcination explains the presence of dispersed NiO nanoparticles peaks found on the surface of the catalysts. This confirms that the decrease in pore volume and specific surface area of doped catalyst supports is due to the impregnated NiO nanoparticles. The XRD pattern of 5 wt% Pd/Al_2O_3 catalyst showed alumina peaks at about $2\theta = 45.7°$ and 67°, whereas Pd metals peaks appeared around 32° and 40.2°, respectively. The average crystallite sizes of the impregnated NiO metal were 22.44 ± 0.05 nm (30 wt% Ni/SiO_2), 19.56 ± 0.11 nm (30 wt% Ni/ZrO_2-SiO_2), and 40.38 ± 0.53 nm (30 wt% Ni/$NbOPO_4$), and for Pd metal supported on Al_2O_3 it was12.47 ± 6.13 nm. There were no other unknown peaks suggesting that the prepared support materials are of an excellent purity.

3.1.3. Catalyst acid sites type, number, and strength

The recorded pyridine-FTIR spectra to identify different types of acidic sites based on the adsorbed pyridine by the catalysts is shown in Fig. 4. The quantification of the strength of the identified acid site type is presented in Table 2. From the results, three different acid sites can be observed and identified based on the pyridine-FTIR spectra (Fig. 4**b**). These correspond to weak acid, moderate acid, and strong acid sites. From Table 2, the concentration of the moderate acid sites is higher than that of the weak (Lewis) and strong (Brønsted) acid sites. The Lewis acid sites (Lewis-bonded pyridine) on the catalysts surface can be observed from the adsorption IR spectra of pyridine at peak wavenumber 1444 cm^{-1}, the peak at wavenumber 1540 cm^{-1} corresponded to the Brønsted acid sites (Brønsted-bonded pyridine), and the peak at wavenumber 1490 cm^{-1} was ascribed to the simultaneous adsorption of pyridine on Brønsted and Lewis sites. These observations collaborate with the literature on the identification of acid sites by pyridine-FTIR method [23,25]. The $NbOPO_4$ catalyst and the Ni-doped ones have higher concentration of Lewis acid sites than Brønsted, while for the SiO_2 and ZrO_2-SiO_2 reverse is the case (Table 2). The Brønsted acid sites on the surface of the $NbOPO_4$ can be assigned to the presence of Nb-OH and P-OH groups, while the Lewis acid sites have been reported to result from octahedra NbO_6 and tetrahedra NbO_4 [23]. The results show that the total acid sites strength of the catalysts can be ranked as follows: $NbOPO_4$ > 10 wt% Ni/$NbOPO_4$ > 30 wt% Ni/$NbOPO_4$ > 5 wt% Pd/Al_2O_3 > 30 wt% Ni/ZrO_2-SiO_2 > 30 wt% Ni/SiO_2 (Table 2). Thus, $NbOPO_4$ catalyst has the highest acidity among the catalysts that were developed, while 30 % wt. Ni/SiO_2 has the lowest. Notably, the strength of the Lewis acid sites decreases from 39.4 to 26.6mmol g^{-1} and the Brønsted acid sites from 23.5 to 16.0mmol g^{-1} as the doping of $NbOPO_4$ with NiO increases from 0 to 30 wt% (Table 2).

The actual Ni metal content in the prepared catalysts based on ICP-OES technique results range from 27.3 to 29.6 wt%, with an average of 28.5 ± 1.1 wt%.

Table 1
Catalyst support materials textural properties.

Support materials	Average pore diameter (nm)	Pore volume (cm^3/g)	Surface area (m^2/g)
Synthesized support materials			
SiO_2	5.00	0.42	197
ZrO_2-SiO_2	9.85	0.62	224
$NbOPO_4$	3.43	0.47	411
Supported metal catalysts			
30 wt% Ni/SiO_2	8.42	0.21	53.1
30 wt% Ni/ZrO_2-SiO_2	8.34	0.32	92.9
30 wt% Ni/$NbOPO_4$	3.41	0.35	125
5 wt% Pd/Al_2O_3	7.96	0.27	90.2

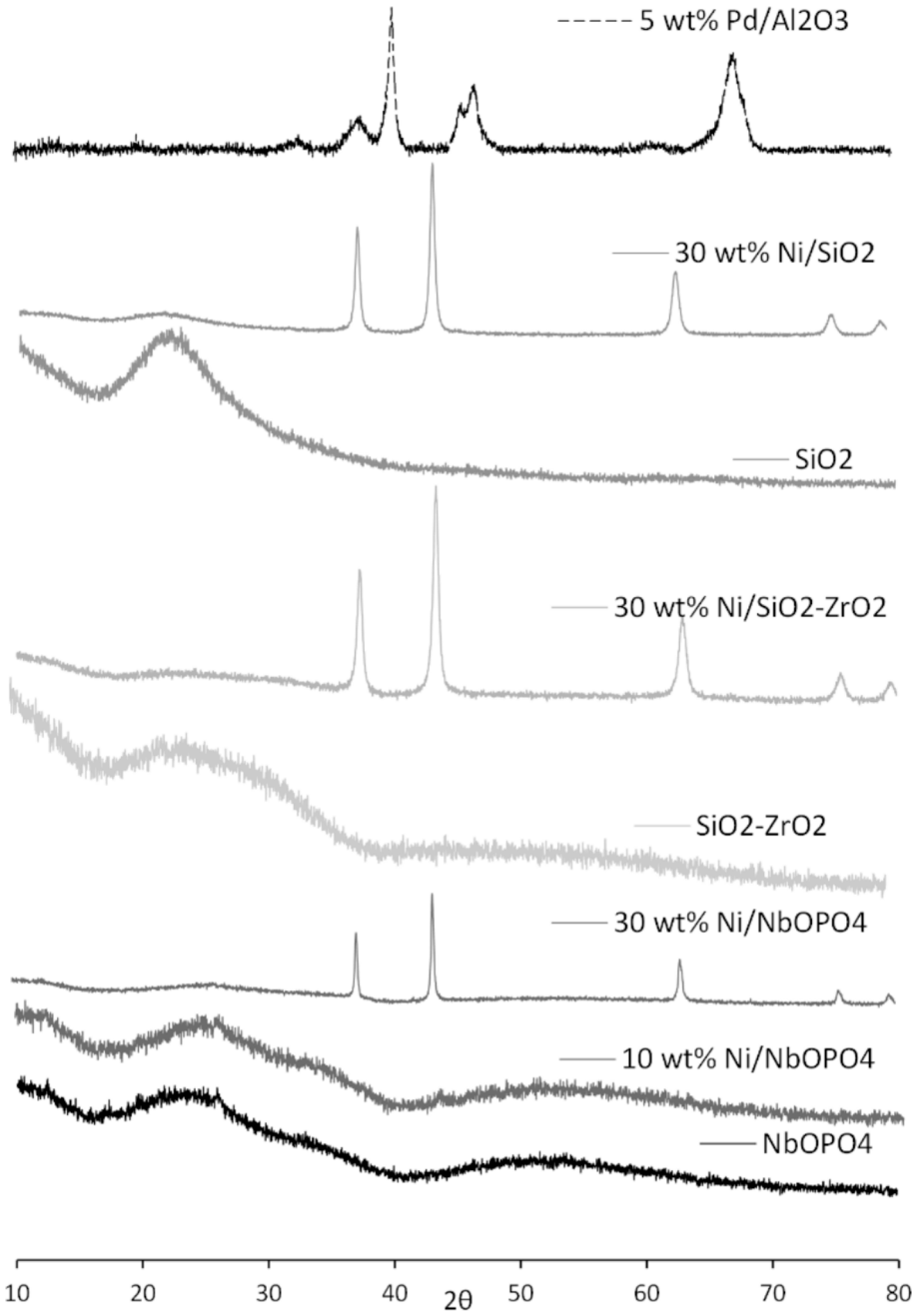

Fig. 3. XRD diffraction patterns of the fresh catalysts.

3.2. Results from two-pot approach involving the first-stage aldol condensation followed by second-stage hydrogenation are discussed in this section

3.2.1. Effect first-stage reaction medium

Table 3 shows the influence of reaction time on selectivity of products and conversion of 10 g cyclohexanone during the first stage of the two-pot approach. Here, cyclohexanone was reacted at 160 °C for 1 h to 3 h reaction times in the presence of 0.5 g of $NbOPO_4$ and 5 bar of initial hydrogen gas pressure. The results show that the conversion of cyclohexanone increased, notwithstanding almost marginally, with increasing reaction times at 160 °C as follows: 60 % (1 h), 66.32 % (2 h) and 68.4 % (3 h) under hydrogen atmosphere. Giving that only about 2 % increase in conversion of cyclohexanone occurred when the reaction time was raised from 2 h to 3 h, there was no real incentive to test longer reaction times beyond 3 h in this present study.

Table 3 shows the selectivity of a broad range of products categories into three based on the extent to which C-C coupling occurred or not. These include, (a) compounds with 6 carbon atoms that formed directly from a single cyclohexanone moiety without aldol condensation, hereby known as "No C-C condensation" products, (b) compounds with mostly 12 carbon atoms formed from the C-C coupling of only two cyclohexanone moieties, hereby denoted as "Single C-C condensation" products, and (c) compounds with mainly 16——18 carbon atoms formed from the C-C coupling of more than two cyclohexanone moieties; these are designated as "2 + C-C condensation" products. The C-C coupled products included the adduct 1′-hydroxy-[1,1′-bicyclohexyl]-2- one, which could undergo in-situ dehydration, producing two observed isomeric products, such as 2-(1-cyclohexen-1-l)cyclohexanone and 2-cyclohexylidencyclohexanone as shown in **Reaction** Scheme 1.

Table 3 shows that the $NbOPO_4$ was able to produce high yields of single C-C couple aldol condensate products (Supplementary

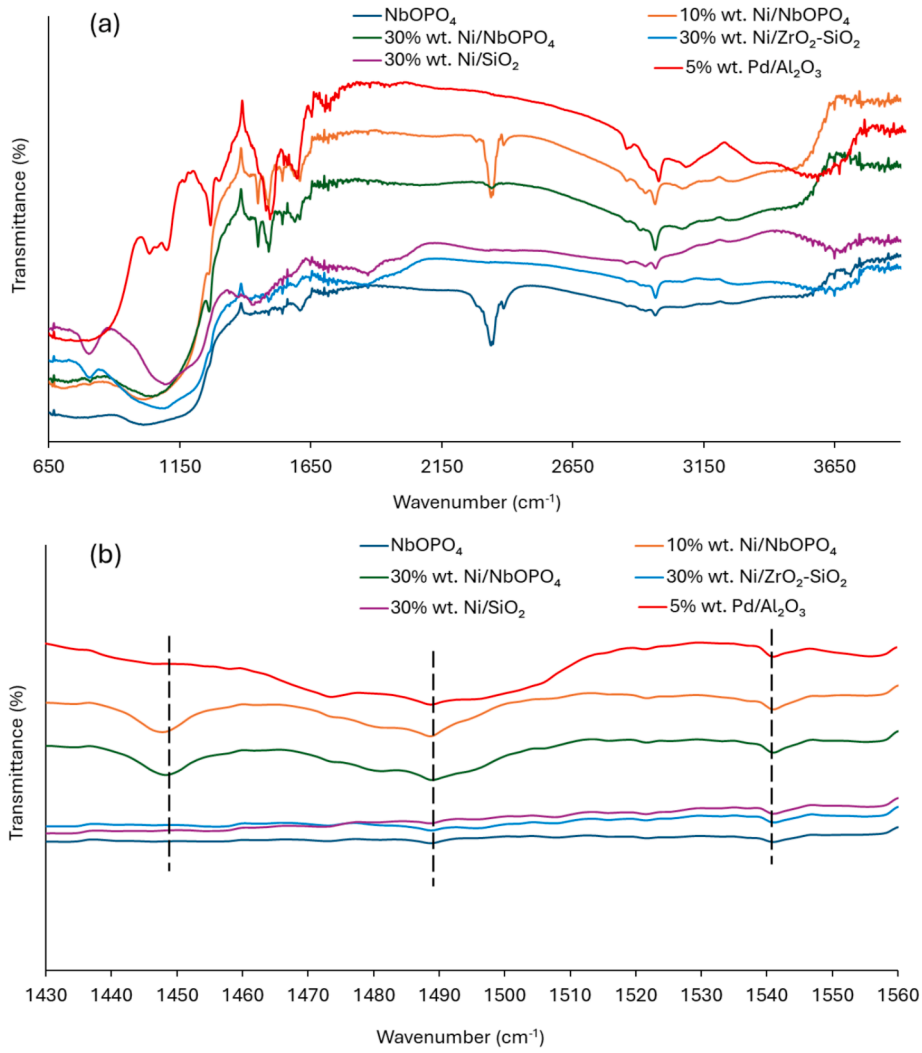

Fig. 4. Pyridine-FTIR spectra of the different catalysts: (a) full range spectra scan and (b) pyridine adsorbed acid sites spectra range.

Table 2
Semi-quantitation of acid site types and strengths for the different catalysts based on pyridine-FTIR.

Type of acid site	Peak position wavenumber (cm^{-1})		
Lewis	1444		
Bronsted	1540		
Lewis + Bronsted	1490		
Strength of acid sites (mmol g^{-1})			
Catalyst	Lewis	Bronsted	Lewis + Bronsted
$NbOPO_4$	39.4	23.5	68.2
10 wt% Ni/$NbOPO_4$	33.0	19.7	58.0
30 wt% Ni/$NbOPO_4$	26.6	16.0	47.9
30 wt% Ni/ZrO_2-SiO_2	0.84	9.15	10.0
30 wt% Ni/SiO_2	1.11	7.73	8.49
5 wt% Pd/Al_2O_3	8.44	17.5	26.4

Information Tables S1). Although, reaction after 1 h gave the highest selectivity for desirable single C-C coupling condensates, the conversion of cyclohexanone was lowest at about 60 % under hydrogen. It appeared that the results after 3 h reaction time were more useful for producing precursors of components of aviation fuel i.e., rich in C_{12} compounds with lower C_{18} adducts. In other words, 3 h gave both the increased conversion of cyclohexanone (68.4 %) and the lower selectivity towards 2 + C-C condensation products compared to the results obtained after 2 h. Hence, the 3 h reaction time was used to produce the first-step liquid

Table 3
Cyclohexanone conversion and C-C coupling products selectivity at temperature of 160 °C, 10 g cyclohexanone, 0.5 g $NbOPO_4$ catalyst loading and 10 bar initial hydrogen pressure.

Conversion and product	Reaction time		
	1 h	2 h	3 h
Cyclohexanone conversion (%)	60.0	66.3	68.4
No C-C condensation oxygenates selectivity (%)	0.0	0.16	0.0
Single C-C condensation oxygenates selectivity (%)	65.8	63.3	59.2
2 + C-C condensation oxygenates selectivity (%)	21.3	24.9	28.3
Hydrocarbons selectivity (%)	12.9	12.3	11.9

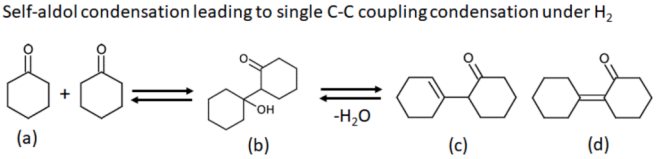

Scheme 1. Reaction Scheme 2. Self-aldol condensation followed by dehydration and hydrogenation reaction [Note: (a) cyclohexanone, (b) 1′- hydroxy-[1,1′-bicyclohexyl]-2-one, (c) 2-(1-cyclohexen-l-yl)cyclohexanone, (d) 2-cyclohexylidenecyclohexanone.

products for the second step operated at 300 °C for HDO. Notably, reaction time has no appreciable effect on the selectivity towards deoxygenated hydrocarbon products, with results within a similar average. Similarly, dimeric bicyclo-oxygenates as well as monomeric, dimeric, trimeric, and tetrameric cyclic hydrocarbons have been produced from a similar cyclic ketone [27]. In that study, aldol condensation of cyclopentanone over Cu/Al_2O_3 catalyst at 1 MPa hydrogen, 280 °C temperature, and 2 h-1 wt hourly space velocity (WHSV) [27]. However, in this present study, the high-density adduct intermediates were produced at a much lower aldol condensation temperature of 160 °C.

3.2.2. *Effect of catalyst types on second stage reaction during two-pot approach*

Since the products of aldol condensation in the first stage still contain a high proportion of oxygenates and/or unsaturated compounds, further treatment was needed to meet the requirements for aviation fuel by solvent-free hydrodeoxygenation (HDO). Table 4 shows the distribution of products from the HDO stage using the supported metal catalysts (30 wt% $Ni/NbOPO_4$,5 wt% Pd/Al_2O_3, 30 wt% Ni/SiO_2, 30 wt% Ni/ZrO_2-SiO_2). The results showed the catalysts led to further conversion of the remaining cyclohexanone carried over from the first step. Clearly, only small amounts (<2 wt%) of the cyclohexanone remained when 30 wt% $Ni/NbOPO_4$ and 5 wt% Pd/Al_2O_3 were used as HDO catalysts, whereas the liquid products obtained with 30 wt% Ni/SiO_2 > 30 wt% Ni/ZrO_2-SiO_2 still contained about 15 % − 20 % of the feedstock.

The compounds (i.e., excluding cyclohexanone) observed in the second-stage liquid products were classified into oxygenates and hydrocarbons and there selectivities shown in Table 4. Results in Table 3 show that the catalytic activity based on overall cyclohexanone conversion were as follows: 30 wt% $Ni/NbOPO_4$ > 5 wt% Pd/Al_2O_3 > 30 wt % Ni/SiO_2 > 30 wt% Ni/ZrO_2-SiO_2. Similar trend was observed with the yield of hydrocarbons, corresponding to the ability of the catalyst to perform hydrodeoxygenation (HDO) and dehydration. Therefore, the yields of hydrocarbons implied that 30 wt% $Ni/NbOPO_4$ catalyst exhibited better HDO activity, followed by 5 wt% Pd/Al_2O_3 whereas 30 wt% Ni/ZrO_2-SiO_2 demonstrated worse HDO activity. This trend of selectivity towards hydrocarbons is consistent with the catalyst ranking as observed in Table 2 based on the strength of the acid sites.

Literature have reported that the primary C-O bond cleavage in oxygenated organics process takes place on acid catalytic sites, resulting in dehydration of the oxygenates reaction intermediates [3]. Hence, the primary mechanisms involved in the HDO of oxygenates obtained from the aldol condensation has been identified in the literature as being dehydration, followed by hydrogenation [3]. In addition to the dehydration reaction leading to loss of water, oxygen was removed from the reaction intermediates in form CO and CO_2, based on the composition of the produced gas. The high activity of the Ni supported $NbOPO_4$ catalyst could be attributed to its larger surface area and higher acid sites (Tables 1 and 2). This implied the acid sites of Ni supported on SiO_2 and ZrO_2-SiO_2 catalysts are too weak to activate dehydration and hydrodeoxygenation reactions relative to $NbOPO_4$ material [30]. Therefore, the strong Brønsted and Lewis acid sites of $NbOPO_4$ produced a superior HDO activity and outperformed the moderate Lewis acid site Al_2O_3 and ZrO_2-SiO_2, and weak acid sites of SiO_2 support materials [20,31,32]. The observation aligns with the acid sites type and strength reported in Table 2.

Therefore, due to the poor performances of 30 wt% Ni/SiO_2 and 30 wt % Ni/ZrO_2-SiO_2 catalysts during the HDO tests, details of the compositions of the liquid products obtained from them are not discussed further. The compositions of the liquid products from GC/MS analysis can be found in the Supplementary Information Tables S2-S4. Instead, efforts hereafter have focused on the detailed compositions of the products obtained from the use of 30 wt% $Ni/NbOPO_4$ and 5 wt% Pd/Al_2O_3 as HDO catalysts. The distribution of hydrocarbon products exhibited carbon number in the range of C_6 to C_{18}, which were classified as follows: **(1)** naphthenes (e.g., cyclopentane, cyclohexane, 1,1′-bicyclohexyl, cyclopentylcyclohexane, etc.); **(2)** alkyl naphthenes (e.g., methyl-cyclopentane, methyl-cyclohexane, pentyl-cyclohexane, cyclopentyl-cyclohexane, etc.); **(3)** alkyl aromatics (e.g., pentyl-benzene, toluene, cyclohexyl-benzene, p-dicyclohexylbenzene, benzylcyclopentane, etc.); **(4)** partially hydrogenated polyaromatics (e.g., 1,2,3,4-tetrahydro-naphthalene ($C_{10}H_{12}$), [3-(2-cyclohexylethyl)-6-cyclopentylhexyl]-benzene, 5-ethyl-1,2,3,4-tetrahydro-naphthalene ($C_{12}H_{16}$), 1,2,3,6,7,8-hexahydro-as-indacene ($C_{12}H_{14}$), 1,2,3,4,5,6,7,8,9,10,11,12-dodecahydro-triphenylene ($C_{18}H_{24}$), 1,2,3,4,5,6,7,8-octahydrotriphenylene ($C_{18}H_{20}$), etc.), and **(5)** polyaromatic (e.g., naphthalene, 2-methyl-naphthalene, 2-ethyl-naphthalene, phenanthrene, 1,2,3,4-tetrahydro-triphenylene ($C_{18}H_{16}$), triphenylene, etc.). A detailed products distribution can be found in the supplementary information Tables S2-S4.

The selectivity of hydrocarbon products in the produced liquid fuel using 30 wt% $Ni/NbOPO_4$ and 5 wt% Pd/Al_2O_3 catalysts for HDO of the aldol products at a reaction temperature of 300 °C, initial hydrogen pressure of 10 bar, and reaction duration of 3 h and 6 h is shown in Fig. 5. For Fig. 5a, the results demonstrated that the selectivity of hydrocarbon products in the produced fuel with 30 wt% $Ni/NbOPO_4$ catalyst was as follows: alkyl aromatics (39 %) > partially hydrogenated polyaromatics (23 %), naphthenes (18 %) > alkyl naphthenes (11 %) > polyaromatics (3.4 %). In contrast, with the 5 wt% Pd/Al_2O_3 catalyst, there is a notable increase in selectivity towards naphthenes (35.6 %) and alkyl aromatics (35 %). Since naphthenes (mono- and bicycloalkanes), alkyl aromatics, and polyaromatic hydrocarbons were all formed during the HDO of aldol products, dehydrogenation and hydrogenation was assumed to occur in competition [33].

It is worth noting that cyclic hydrocarbons (single ring naphthene C_5-C_6) could have been produced mostly from the cyclohexanone via hydrogenation on the catalyst active sites. The observed single ring naphthenic and single ring aromatic hydrocarbons included 1-methylcyclopentane, cyclohexene, cyclohexane, 3-methylcyclopentane, methylcyclohexane, and methylcyclopentene, as well as toluene and phenol. These arrays of observed products must have resulted from the combination of hydrogenation, dehydrogenation, and dehydration reactions demonstrated by the reaction network shown in **Reaction** Scheme 2. The acidic site of catalyst carries out dehydration functionality, while the metallic active site performs hydrogenation and dehydrogenation reactions. For instance, cyclohexanone could be hydrogenated into cyclohexanol, which would undergo dehydration to cyclohexene, and then, dehydrogenation to phenol or hydrogenation to cyclohexane.

The formation of C_5 compounds indicated decarbonylating, followed by a series of reactions such as 2,5 carbon linkages to form cyclopentane, ring-opening reactions to form n-pentane, cleavage of C-C bonds in the n-pentane to form C_1 – C_4 species. Together with n-pentane, the C_1 – C_4 species could generate C_1 – C_5 alkyl groups from the alkylation of cyclic compounds to produce alkyl naphthene and aromatic, such as methyl-cyclopentane and pentyl-cyclohexane. This would explain the formation of C_6 to C_{11} hydrocarbons that were observed in the liquid products. More alkylated naphthene and aromatic were produced by 30 wt% $Ni/NbOPO_4$ catalyst compared to 5 wt% Pd/Al_2O_3 catalyst. This suggests that the former was able to perform alkylation reaction in addition to hydrogenation functionality. The inferior alkylation of 5 wt% Pd/Al_2O_3 is evident in Fig. 5**a**. The identified monocyclic hydrocarbon products

Table 4
Conversion and selectivity of compounds in the liquid products obtained from catalytic HDO of first-step liquid products at temperature 300 °C and initial hydrogen pressure of 10 bar for 3 h (first-step aldol condensation of cyclohexanone under hydrogen for 3 h).

Catalyst	Conversion (%)	Oxygenates (%)	Hydrocarbons (%)
30 wt% $Ni/NbOPO_4$	98.9	6.11	93.9
5 wt% Pd/Al_2O_3	98.4	28.0	72.0
30 wt% Ni/ZrO_2-SiO_2	79.9	72.2	27.8
30 wt% Ni/SiO_2	85.7	60.2	39.9

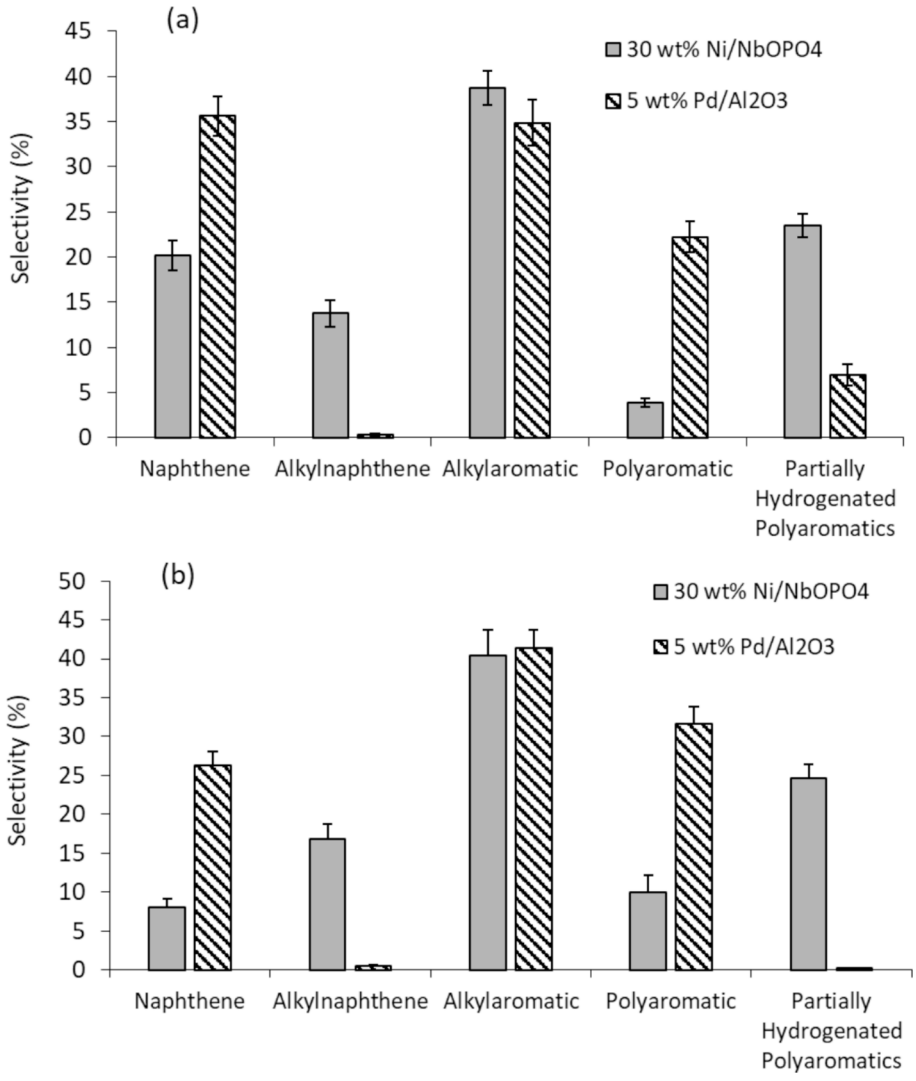

Fig. 5. Effect of 30 wt% $Ni/NbOPO_4$ and 5 wt% Pd/Al_2O_3 catalysts on the distribution of hydrocarbon products in the second step (a) reaction time of 3 h; (b) reaction time of 6 h; at reaction temperature of 300 °C, initial hydrogen pressure 10 bar, and 0.5 g catalyst loading.

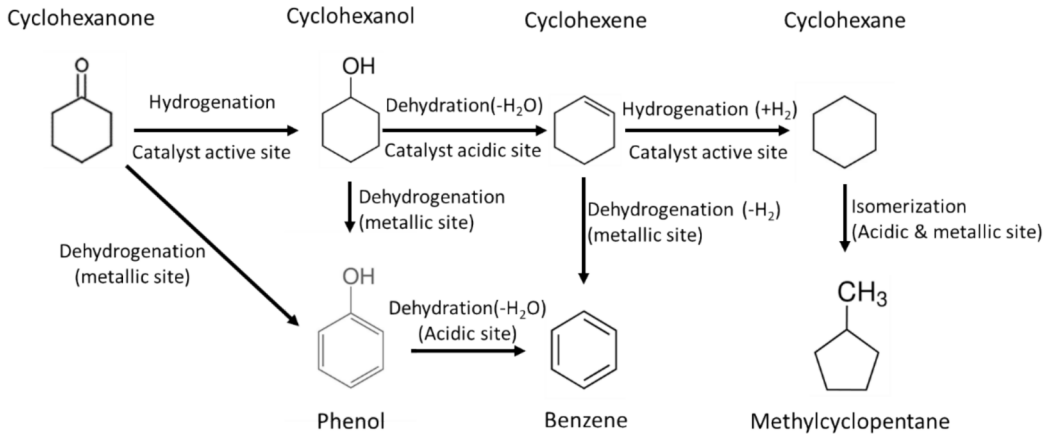

Scheme 2. Pathways to the formation of C_6 cyclic hydrocarbons from cyclohexanone.

have been reported in the literature during the HDO of cyclohexanone into fuel-range products using alumina-supported NiMo and CoMo catalysts at 300 °C [18,34]. HDO, alkylation and isomerisation reactions are catalysed on both acidic and metallic sites of the catalysts [34].

Bicyclic naphthenic (bi-cycloalkanes) hydrocarbons originated from the self-aldol condensation of the cyclohexanone, producing mostly C_{12} hydrocarbons as illustrated in **Reaction** Scheme 3. However, some C_{10} and C_{11} cyclic compounds were also observed and were possibly formed

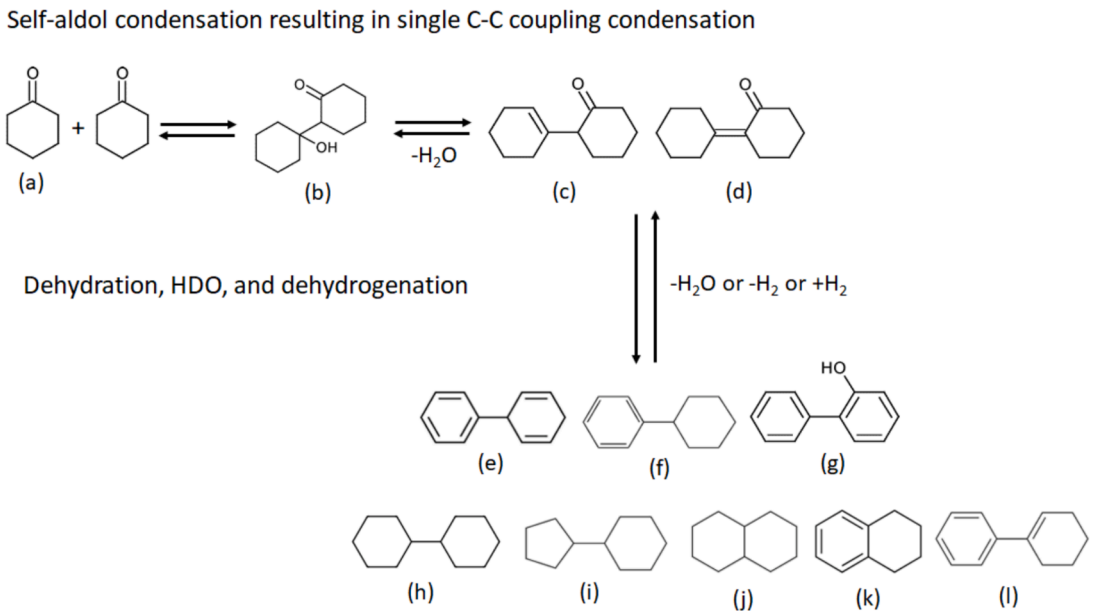

Scheme 3. Self-aldol condensation followed by dehydration and hydrogenation reaction [Note: (a) cyclohexanone, (b) 1′- hydroxy-[1,1′-bicyclohexyl]-2-one, (c) 2-(1-cyclohexen-l-yl)cyclohexanone, (d) 2-cyclohexylidenecyclohexanone, (e) 1,3-cyclohexadienyl-Benzene, (f) cyclohexyl benzene, (g) *o*-Phenyl-phenol, (h) 1,1′-bicyclohexyl, (i) cyclopentylcyclohexane, (j) decalin, (k) $C_{10}H_{12}$, and (l) 1-phenyl-cyclohexene].

from alkylated C_5 – C_6 cyclic hydrocarbons. The bi-cycloalkanes are aviation fuel range high-density compounds with high volumetric heat and thermal stability [9,35]. They included 1,1′-bicyclohexyl, 2-methyl-*trans*-decalin and cyclopentylcyclohexane which are produced from the dehydration, rearrangement, and hydrogenation of the two isomeric mixture of aldol condensation products 2-(1-cyclohexen-1-l)cyclohexanone and 2-cyclohexylidencyclohexanone from the first stage reaction at 160 °C. These compounds are analogous to the high-density fuel-range C-C coupled bicycloalkanes obtained from HDO of adducts derived from cyclopentanone aldol condensation using Ni-SiO_2 and MgAl hydrotalcite catalysts [4,35]. For 30 wt% Ni/$NbOPO_4$ and 5 wt% Pd/Al_2O_3 catalysts, the selectivity towards cycloalkanes, alkyl cycloalkanes, and bi-cycloalkanes was 33.8 % and 36 % respectively. It is well known that hydrogenation occurs on active metals in a bifunctional catalyst. Hence, the results indicated that the hydrogenation activity of 30 wt% Ni/$NbOPO_4$ catalyst was higher than that of 5 wt% Pd/Al_2O_3. Notably, the $NbOPO_4$ alone already facilitated the dehydration and dehydrogenation of some of single C-C couple dimers of cyclohexanone, which are 2-(1-cyclohexen-1-l)cyclohexanone and 2-cyclohexylidencyclohexanone into cyclohexyl-benzene in step 1 as shown in **Reaction** Scheme 1.

It has also been demonstrated that multiple C-C coupling can occur with $NbOPO_4$ catalyst resulting in the formation of polyaromatic hydrocarbons in the first stage, which resulted in hydrocarbon chain in the range of C_{16} to C_{18} as shown in **Reaction** Scheme 4. The metal sites provided in 5 wt% Pd/Al_2O_3 catalyst was ineffective toward hydrogenation of polyaromatics. Whereas the hydrogenation functionality of Ni

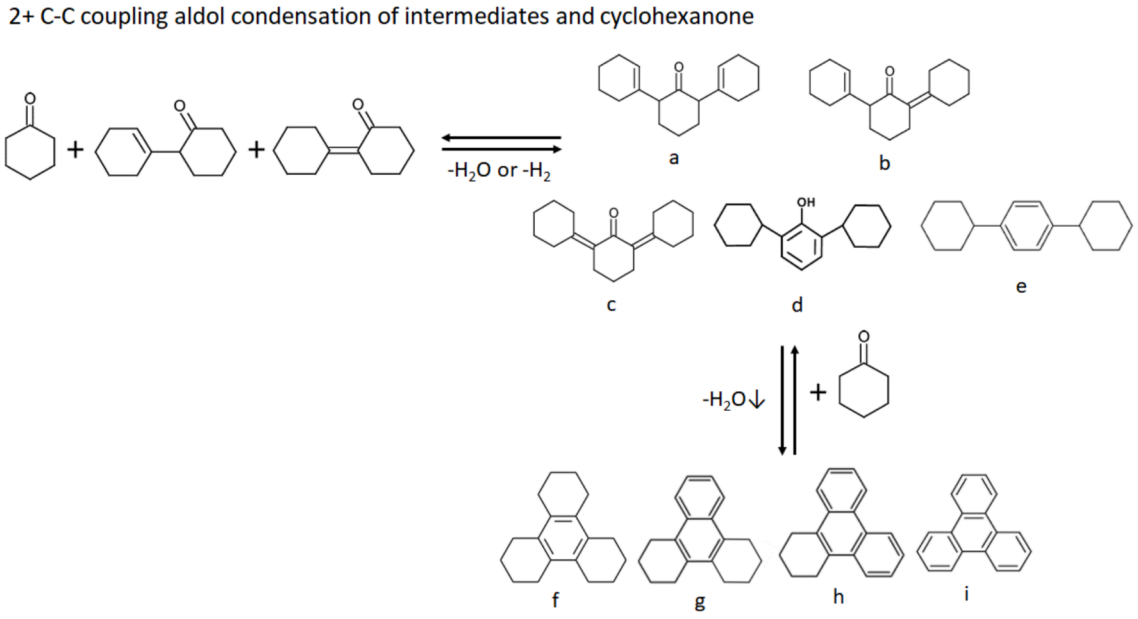

Scheme 4. The pathways to polycyclic hydrocarbons [Note: (a) 2,6-di(1-cyclohexenyl)cyclohexanone, (b) 2-cyclohexylidene,6-(1-cyclohexenyl)cyclohexanone, (c) F3 = 2,6-dycyclohexylidenecyclohexanone, (d) 2,6-dicyclohexylphenol, (e) p-dicyclohexylbenzene, (f) $C_{18}H_{24}$, (g) $C_{18}H_{20}$, (h) $C_{18}H_{16}$, and (i) triphenylene].

metal in the 30 wt% Ni/$NbOPO_4$ catalyst was evident from the production of partly hydrogenated polyaromatic products such as $C_{12}H_{16}$, 1,2,2a,3,4,5-hexahydroacenaphthylene ($C_{12}H_{14}$), $C_{18}H_{24}$, and $C_{18}H_{20}$ (Tables S2-S4). Similar spectrum of hydrocarbons such as monomer, dimer, and trimer cyclic hydrocarbons have been produced from the HDO of aldol condensation adducts of cyclopentanone over 0.1 g Cu/Al_2O_3 catalyst at 1.0 MPa H_2 pressure and 280 °C reaction temperature [26].

Fig. 5b shows the effect of extending the HDO reaction time to 6 h. The selectivity of hydrocarbon products from the hydrogenation stage for both 30 wt% Ni/$NbOPO_4$ and 5 wt% Pd/Al_2O_3 catalysts as a function of time is shown in Fig. 5**b**. While naphthenic hydrocarbons decreased as the reaction time increases from 3 to 6 h, the alkylation of naphthene and aromatic, the synthesis of polycyclic aromatic, and the hydrogenation of polyaromatic into partially hydrogenated polyaromatic hydrocarbons increased when 30 wt% Ni/$NbOPO_4$ catalyst was used (Fig. 5**b**). Whereas with 5 wt% Pd/Al_2O_3 catalyst, both naphthenic and hydrogenation of polyaromatic into partially hydrogenated polyaromatic hydrocarbons decrease as the reaction time increased from 3 to 6 h, producing higher alkyl aromatic and polyaromatic hydrocarbons (Fig. 5**b**). The extremely low levels of alkyl naphthene products in Fig. 5b for 5 wt% Pd/Al_2O_3 catalyst confirmed that 30 wt% Ni/$NbOPO_4$ performed better for naphthene alkylation and hydrogenation of polyaromatic. Notably, when the reaction time was increased from 3 to 6 h, the hydrogenation functionality of 5 wt% Pd/Al_2O_3 catalyst became poorer compared to 30 wt% Ni/$NbOPO_4$, suggesting the deactivation of the catalyst's sites. This could possibly be due to the presence of water from the dehydration reaction that formed hydrocarbons. It has been reported that the deactivation by hydrolysis of alumina to form boehmite AlO(OH) was responsible for the loss of its hydrogenation catalytic activity [36,37].

3.3. One-pot sequential aldol condensation followed by HDO with 30 wt % Ni/$NbOPO_4$

This section describes an alternative method for the combined aldol condensation and the hydrogenation of the resultant adducts into a one-pot process. The one-pot aldol condensation–hydrogenation reaction with two steps could be potentially less labour intensive in batch operation, safe, and cost-effective. It involved no transfer of materials between two reactors and less energy requirement due to elimination of cooling and reheating steps associated with the two-pot approach. Since the two-pot approached showed that 30 wt% Ni/$NbOPO_4$ was overall more effective than 5 wt% Pd/Al_2O_3 during HDO at the second step, $NbOPO_4$, 10 wt% Ni/$NbOPO_4$ and 30 wt% Ni/$NbOPO_4$ catalysts were therefore used in this one-pot approach.

Fig. 6 shows the conversion of cyclohexanone and the C-C coupling hydrocarbon products from these experiments using the same categorisation of compounds explained in Section 3.2. Detailed list of compounds from GC–MS analysis results can be found in the **Supplementary Information** Tables S5-S6. Fig. 6 shows that with the undoped $NbOPO_4$ catalyst, 100 % cyclohexanone conversion was accomplished while for the 10 wt% Ni/$NbOPO_4$ and 30 wt% Ni/$NbOPO_4$ catalysts, approximately 99 % conversion was achieved. In comparison with the conversion observed in Table 4, this indicated that in the second stage of hydrogenation at 300 °C temperature, the unconverted cyclohexanone during the first stage at 160 °C further underwent C-C coupling, hydrogenation, and/or dehydration resulting in increased conversion. The observed results aligned with the works of Shao et al. [38] and Mahajan et al. [39], who reported over 90 % conversion of aldehydes and ketones at high temperatures (> 230 °C), indicating that aldol condensation could benefit from a relatively high temperature. The components of liquid products from these experiments were hydrocarbons with carbon numbers ranging from C_6 to C_{18}. In all cases, the cyclohexanone that survived the aldol condensation became mostly hydrogenated to C_6 hydrocarbons at 300 °C.

Among the three catalysts, the results shows that 10 wt% Ni/$NbOPO_4$ catalyst produced hydrocarbon products with the highest selectivity (48.4 %) toward single C-C condensation product, while 30 wt% Ni/$NbOPO_4$ catalyst produced the highest selectivity toward hydrocarbon products without condensation. This was because with 30 wt % Ni/$NbOPO_4$ the hydrogenation of cyclohexanone into cyclohexanol was highest. The yields of 2 + C-C condensation hydrocarbon products were approximately the same for the three-catalysts investigated. The increased active Ni metal content from 10 wt% to 30 wt% could have decreased the acid site strength of the $NbOPO_4$, thereby increasing the hydrogenation functionality over its C-C coupling activity. Such observation is consistent with the results reported in Table 2, which show that $NbOPO_4$ acidity tends to decrease as Ni content increases. A similar trend of C-C coupled products have been reported in the literature for analogous cyclic ketone molecule cyclopentanone (8 mL) in n-pentane solvent (volume ratio of 1:2) for one-pot aldol condensation (170 °C) followed by HDO (270 °C) over 2.4 g Ni/Mg-Al-O/AC bifunctional catalyst [11].

Fig. 7 shows the selectivity distribution of the hydrocarbons in the liquid products from the one-pot approach. The major hydrocarbon

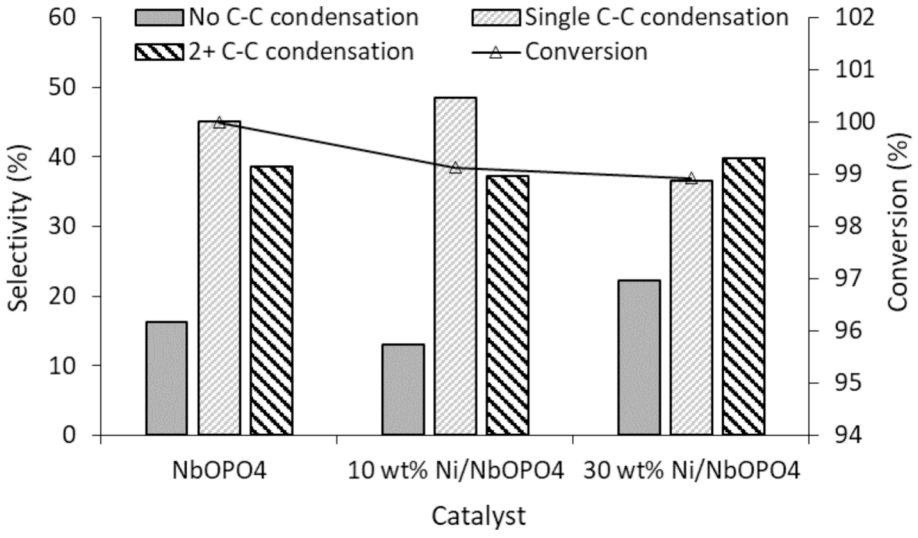

Fig. 6. One-pot aldol condensation reaction and hydrogenation for the different catalyst at 10 bar initial hydrogen pressure, 0.5 g catalyst, 10 g cyclohexanone: initial step = 160 °C for 3 h, and then raised to 300 °C for 3 h.

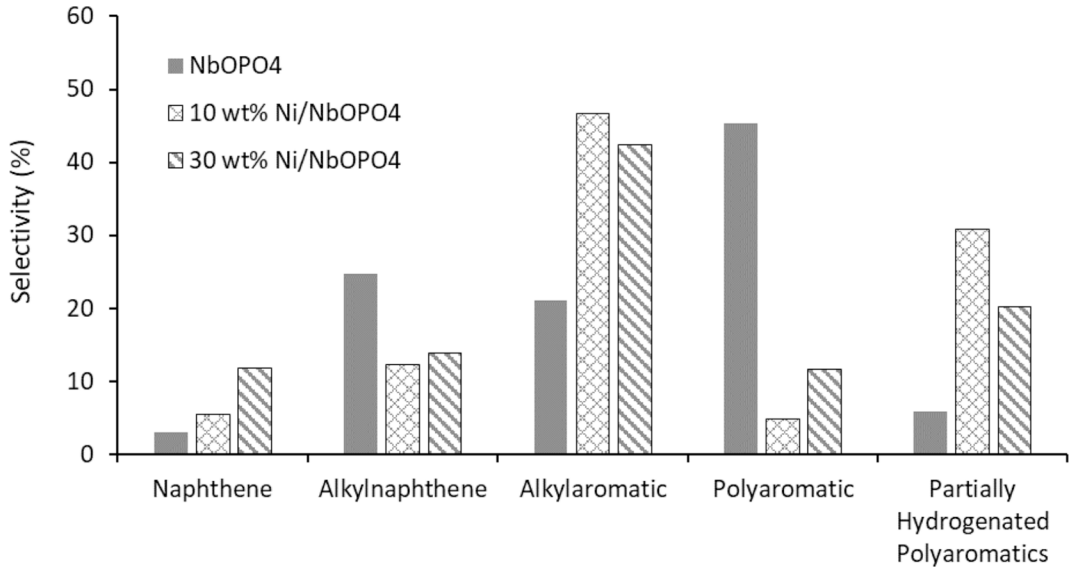

Fig. 7. Hydrocarbon selectivities during one-pot aldol condensation (160 °C for 3 h) followed by high temperature HDO (300 °C for 3 h) at 10 bar initial hydrogen pressure, 0.5 g catalyst, and 10 g cyclohexanone.

product in the liquid products was cyclohexyl benzene, an alkyl aromatic (Tables S5-S6). The results show that the selectivity towards naphthenic hydrocarbon increased as the Ni content of the $NbOPO_4$ catalyst increased from 0 to 30 wt%. In addition, when the Ni content of $NbOPO_4$ increased from 0 to 30 wt%, the alkylation of aromatic increased and the alkylation of naphthene (cycloalkanes) declined. The results show that the Ni supported $NbOPO_4$ catalyst can retain its catalytic activity from the aldol condensation step to still perform hydrodeoxygenation of the C-C condensed adduct products. For instance, compared to the two-pot approach (Fig. 5a), the use of 30 wt% Ni/$NbOPO_4$ catalyst in this one-pot system produced similar selectivities toward alkyl naphthene, alkyl aromatic and partially hydrogenated polyaromatic. However, in comparison to two-pot approach (Fig. 5**a**), while the yield of naphthene decreased to 11.86 %, the yield of polyaromatic hydrocarbons increased to 11.7 % for one-pot approach.

Consequently, the liquid product obtained with undoped $NbOPO_4$ mostly contained polyaromatic hydrocarbons, including triphenylene, phenanthrene, anthracene, and naphthalene. This can be attributed to the strong acidic sites (Table 2), which promoted condensation followed by subsequent dehydrogenation, and aromatisation of naphthenic rings. Essentially, the presence of Ni suppressed aromatization of naphthenic ring due to decreased acidity, which can be observed in the favourable selectivity toward partially hydrogenated polyaromatic relative to polyaromatic hydrocarbons [14]. Such partially reduced aromatics included $C_{12}H_{16}$, $C_{12}H_{14}$, $C_{18}H_{24}$, and $C_{18}H_{20}$, which were observed in the liquid products when 10 wt% Ni/$NbOPO_4$ and 30 wt% Ni/$NbOPO_4$ were used (Tables S5-S6).

3.4. Coke formation

Enhanced aromatisation of components in the liquid products would result in more coke formation. This hypothesis may be explored further by post-reaction evaluation of the coke deposition on the used catalysts. GC/MS results of liquid products have shown that multiple C-C coupling and dehydrogenation resulted in the formation of polyaromatics, implying plausible condensation into coke as an undesirable side reaction. As a result, the catalyst may experience deactivation due to coke-induced pore obstruction and obscuring of active sites. For fair comparison with the one-pot approach, the recovered catalysts from the HDO (second) stage of the two-pot approach have been used in this study. After reaction, the spent catalysts were subjected to thermogravimetric analysis (TGA) with temperature ramped from 40 °C to 900 °C with air at a flow rate of 30 cm^3/min. This technique allowed the various deposits on the catalyst to burn-off at different temperature ranges.

3.4.1. Coke formation on spent catalysts used during the two-pot approach

The TGA thermograms (TG) and differential thermograms (DTG) for the different catalysts both fresh and spent used in the HDO stage of the two-pot approach are shown in Fig. 8. The fresh catalysts TG and DTG curves indicated no weight loss changes in response to temperature rise (Fig. 8**a**). The loss of moisture within the pores of catalysts accounted for 1.4 wt% to 3 wt% losses. This implied that the catalysts were thermally stable. However, weight loss changes were observed in the spent catalysts as shown in Fig. 8**b**, which can be attributed to the volatilisation and combustion of retained hydrocarbons and coke deposited during the hydrogenation reaction [40]. From the DTG curves, the volatilisation and degradation peak in the temperature range 110 °C–340 °C represented the residuals of several hydrocarbon products especially polyaromatics retained in the spent catalyst. This was consistent with previous research on coke determination by thermogravimetry, which has shown that TG or DTG curves evidently suggested that oil and coke were volatilised and combusted at temperatures ranging from 100 °C to 300 °C and 300 °C to 700 °C, respectively [40,41].

The quantity of retained hydrocarbons in the spent catalysts were as follows: 30 wt% Ni/$NbOPO_4$ (39.42 %), 30 wt% Ni/SiO_2 (24.24 %), 30 wt% Ni/ZrO_2-SiO_2 (21.74 %), and 5 wt% Pd/Al_2O_3 (18.36 %). However, the next peak on the DTG curves, denoting oxidation temperatures in the range 420 °C – 560 °C for 30 wt% Ni/$NbOPO_4$ and 30 wt% Ni/SiO_2 catalysts, 380 °C–450 °C for 30 wt% Ni/ZrO_2-SiO_2, and 414 °C–560 °C for 5 wt% Pd/Al_2O_3 were due to coke burn-off. The resultant coke yields from the different catalysts decreased in the following order: 0.62 wt% (30 wt% Ni/$NbOPO_4$) > 0.49 wt% (5 wt% Pd/Al_2O_3) > 0.2 wt% (30 wt % Ni/ZrO_2-SiO_2) > 0.17 wt% (30 wt%v Ni/SiO_2). The coke contents were considerably low, indicating potential minimal catalyst deactivation from coke formation.

In addition to the strength of the acid sites of 30 wt% Ni/$NbOPO_4$ (Table 2), it also possessed larger surface area than the other catalysts (Table 1); hence, the strong acid sites of $NbOPO_4$ caused excessive C-C coupling, condensation, and dehydrogenation reactions [32], which are pathways to coke formation.

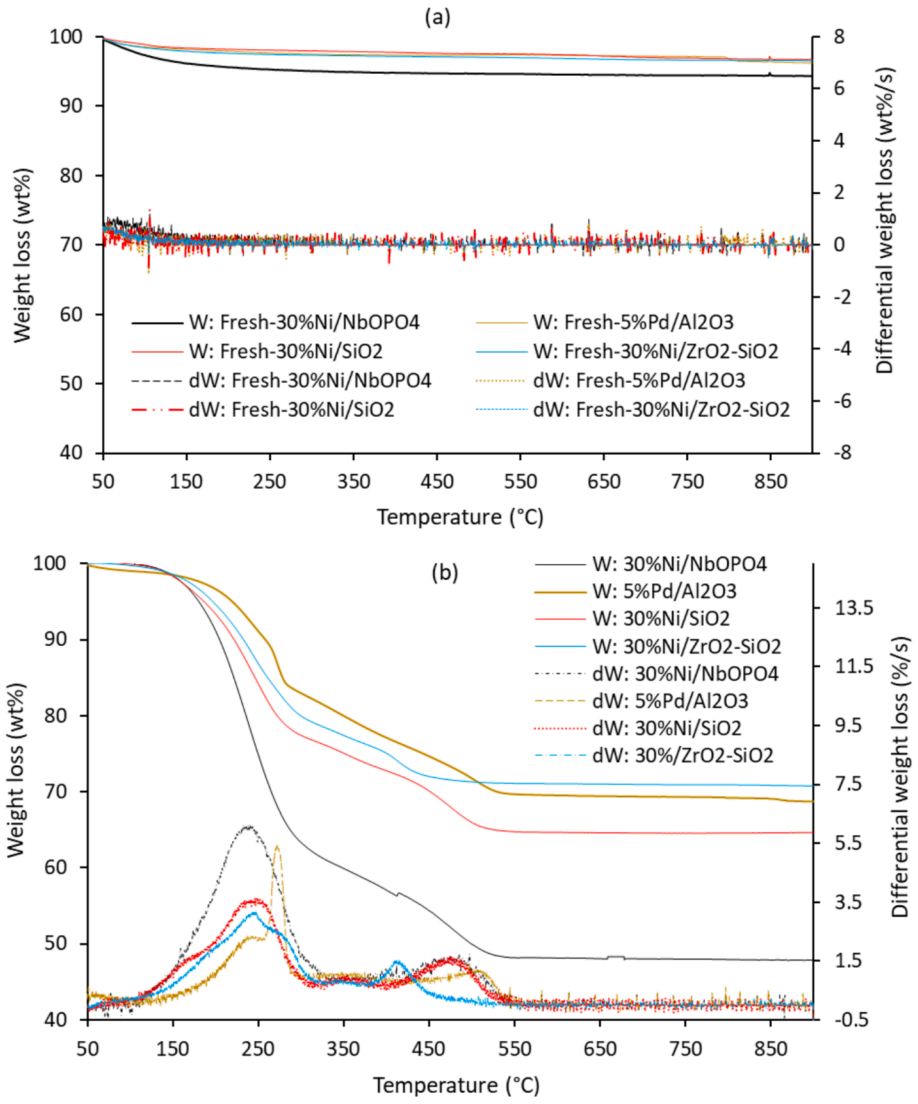

Fig. 8. Thermographs of thermogravimetric (TG) and differential thermogravimetric (DTG) of: (a) fresh catalysts and (b) spent catalysts after hydrogenation adducts at 300 °C temperature, 0.5 g catalyst loading, 10 bar initial hydrogen pressure, and 3 h reaction time using two-pot.

3.4.2. Coke formation on spent catalysts used during the one-pot approach

Fig. 9 shows the TG and DTG curves of the spent catalyst from the one-pot approach, which combined aldol condensation and HDO in one reactor, without first stage sampling. Again, as mentioned in Section 3.3.1, based on the DTG curves, the volatilisation and combustion peak in the temperature range 50 °C–352 °C indicated the residues of various hydrocarbon compounds, particularly polyaromatics, that were retained in the recovered catalyst. However, the second peak region, temperature range 352 °C–656 °C for $NbOPO_4$ and 352 °C–625 °C for the Ni-supported on $NbOPO_4$ catalysts, corresponded to weight loss from coke burn-off.

In comparison to 1.83 wt% coke yield observed when $NbOPO_4$ catalyst was utilised, the incorporation of 10 wt% Ni decreased the coke yield to 1.63 wt%, representing about 11 % reduction in coke formation, while 30 wt% Ni produced further reduction of coke to 1.59 wt%. By adding Ni metal to the $NbOPO_4$, the amount of coke formed became lower, which could extend the lifespan of catalysts. This theory is supported by the large concentration of polyaromatic hydrocarbons, such as triphenylene, phenanthrene, and naphthalene, in the liquid product obtained when undoped $NbOPO_4$ was used. Notably, compared to the two-pot method (Fig. 7), coke yield in a one-pot approach was significantly higher by more than twofold. The coke from the one-pot approach also combusted at a higher temperature indicating that it contained much more condensed coke.

3.5. Gas products

The presence of hydrogen, CO, CO_2 and C_1–C_4 alkanes and alkene gases indicated that in addition to C-C coupling and HDO reactions in the liquid phase, a wide range of other reactions occur. The results for both two-pot and one-pot systems are shown in Table 5. For the two-pot system, the gas yield increase in the same order as the coke yield (Fig. 8), conversion of cyclohexanone, and the selectivity towards hydrocarbons (Table 4). The higher amount of CO plus CO_2 in the produced gas for the two-pot in the presence of 30 wt% Ni/$NbOPO_4$ catalyst was an indication of superior HDO activity than 5 wt% Pd/Al_2O_3 and 30 wt% Ni/SiO_2 catalysts. CO, CO_2, and H_2O have been reported as products of oxygen removal via HDO [42].

The gas product obtained when 5 wt% Pd/Al_2O_3 catalyst was used for the hydrogenation of the adducts were dominated by alkanes, confirming that the Pd promote hydrogenation of olefins. In contrast, 30 wt % Ni/SiO_2 and 30 wt% Ni/$NbOPO_4$ catalyst produced both light alkanes and alkenes gases. The gas formation pathways seem similar between the one-pot and two-pot approached but the latter produced more gas

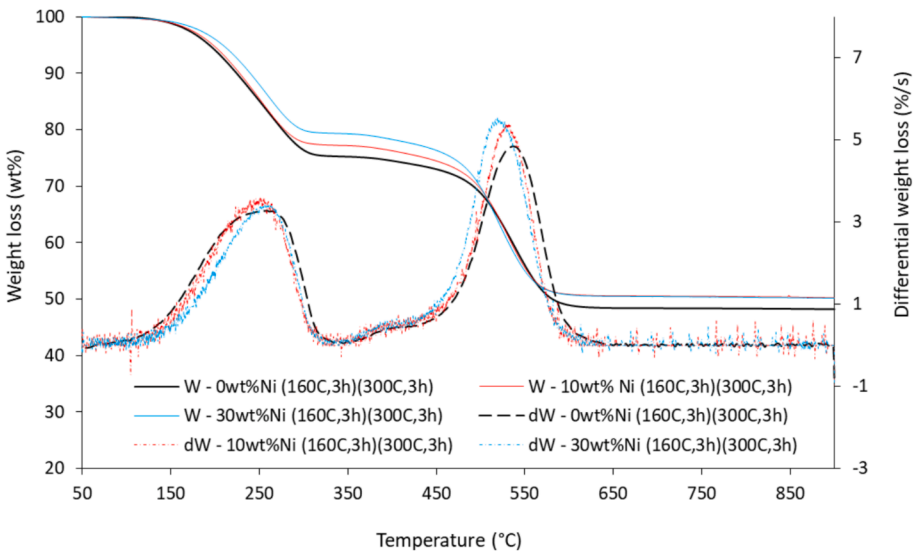

Fig. 9. Thermographs of thermogravimetric (TG) and differential thermogravimetric (DTG) of spent $NbOPO_4$, 10 wt% N/ $NbOPO_4$, and 30 wt% Ni/ $NbOPO_4$ catalysts in a one-pot aldol condensation of cyclohexanone followed by HDO at 160 °C for 3 h and 300 °C for 3 h at an initial hydrogen pressure of 10 bar and 0.5 g catalyst loading.

Table 5
Compositions of gas products obtained from two-pot reactors and one-pot reaction approaches.

Produced gases	Two-pot reactors			One-pot reactor		
	30 wt % Ni/ SiO_2	30 wt% Ni/ $NbOPO_4$	5 wt% Pd/ Al_2O_3	$NbOPO_4$	10 wt% Ni/ $NbOPO_4$	30 wt% Ni/ $NbOPO_4$
CH_4 (wt%)	2.55	0.55	1.74	2.86	0.35	0.60
C_2H_4 (wt %)	0.02	0.024	0.00	0.75	2.96	0.27
C_2H_6 (wt %)	0.09	2.31	0.09	2.47	1.25	2.21
C_3H_6 (wt %)	0.01	0.019	0.00	0.28	0.32	0.16
C_3H_8 (wt %)	0.07	0.11	0.98	1.81	0.22	0.31
C_4H_8 (wt %)	0.001	0.01	0.00	0.92	0.03	0.07
C_4H_{10} (wt %)	0.01	0.081	0.07	0.94	0.43	0.34
CO (wt%)	0.67	1.56	2.85	0.88	0.00	2.95
CO_2 (wt%)	0.47	3.79	2.05	1.48	10.1	4.90
Total gas yield (wt %)	3.87	8.45	7.77	12.4	15.6	11.8

than the former, when comparing the gas yields obtained from the use of 30 wt% Ni/$NbOPO_4$ in both cases.

3.6. Overall mass balances

After cooling the reactor to room temperature at the end of each experiment, the gas product was sampled into a 1 L Tedlar gas bag and analysed on a gas chromatograph capable of separating and quantifying both permanent gases and C_1-C_4 hydrocarbon gases. The permanent gases (H_2, N_2, O_2, CO and CO_2) were detected with a thermal conductivity detector (TCD) while the hydrocarbon gases (methane, ethene, ethane, propene, propane, butenes and butane) were detected with a flame ionisation detector (FID). The chromatographic conditions used for the analysis of gas products have severally been published by the authors [5,39]. The yield of each detected gas component was obtained from ideal gas equation based on the reactor headspace volume and the final pressure of the cooled reactor.

For each experiment, the total yield of gas product was calculated from equation (3).

$$Gasyield, wt\% = \frac{\sum massofgascomponents}{Massofcyclohexanonefeed} \quad (3)$$

After discharging the gas product, the total mass of the reactor and its remaining contents (glass wool, used catalyst, solid product and liquid product) was recorded. The total solid product from each experiment was obtained from two sources; (a) those mixed with the liquid product and recovered by vacuum filtration and (b) as coke on the used catalyst determined by TGA (Section 3.4, with mass losses above 450 °C in Fig. 8 and Fig. 9). Therefore, the solid residue yield was calculated by equation (4).

$$Solidresidueyield, wt\% = \frac{Massofsolidrecoveredbyfiltration + massofcoke}{Massofcyclohexanonefeed} \quad (4)$$

The mass of liquid product from each experiment was determined from the mass of gas-free reactor contents (M_t), the mass of solid products (M_{sp}), the mass catalyst (Mcat) and the mass of volatiles released from the catalysts below 400 °C during TGA. The yield of liquid product was calculated by equation (5).

$$Liquidyield, wt\% = \frac{(M_t - M_{sp} - M_{cat}) + MassofvolatilesfromTGAofusedcatalyst}{Massofcyclohexanonefeed} \quad (5)$$

Table 6 presents the yields of gas, liquid and solid products from each

Table 6
Yields of products and mass balances for one-pot and two-pot reaction systems.

Catalyst	Reactor system	Temperature (°C), time (h)	Solid (wt%)	Gas (wt%)	Liquid (wt%)	Balance (wt%)
$NbOPO_4$	Two-pot, 1st stage	160, 3	0.64 ± 0.16	3.39 ± 0.21	93.6 ± 1.80	97.6 ± 1.70
30 wt%Ni/$NbOPO_4$	Two-pot, 2nd stage	300, 3	0.62 ± 0.11	8.51 ± 0.17	86.2 ± 1.45	95.2 ± 1.44
30 wt%Ni/SiO_2	Two-pot, 2nd stage	300, 3	0.17 ± 0.02	3.91 ± 0.11	92.3 ± 1.22	96.4 ± 1.23
30 wt%Ni/ZrO_2-SiO_2	Two-pot, 2nd stage	300, 3	0.20 ± 0.02	3.94 ± 0.08	92.6 ± 1.03	96.7 ± 1.12
5 wt%Pd/Al_2O_3	Two-pot, 2nd stage	300, 3	0.49 ± 0.04	7.83 ± 0.55	89.6 ± 0.76	97.9 ± 1.17
$NbOPO_4$	One-pot	(160, 3), (300, 3)	1.83 ± 0.10	7.06 ± 0.26	86.0 ± 0.88	94.9 ± 0.96
10 wt%Ni/$NbOPO_4$	One-pot	(160, 3), (300, 3)	1.63 ± 0.21	6.52 ± 0.31	87.4 ± 1.06	95.5 ± 1.54
30 wt%Ni/$NbOPO_4$	One-pot	(160, 3), (300, 3)	1.59 ± 0.18	6.18 ± 0.43	87.8 ± 0.96	95.6 ± 1.08

experiment, along with the mass balance closures of greater 95 wt% or greater. The generally low standard deviations confirm the reproducibility of the experimental procedure used in this work. The liquid products dominated the reaction products in all cases with liquid yields of more than 86 %, followed by gas products. Substantial gas yields were obtained from the experiments involving $NbOPO_4$, the Ni-doped $NbOPO_4$ and the 5 wt% Pd/Al_2O_3. The $NbOPO_4$ and its doped analogues produced the largest yields of solid products, with the one-pot system being more prone to char formation than the two-pot system.

3.7. Preliminary study on the effect of bio-oil components on cyclohexanone conversion

While cyclohexanone can be quantitatively produced from the hydrogenation of phenolic compounds in lignin-derived bio-oils, its isolation before further conversion to sustainable hydrocarbon fuels would increase processing costs. In this part of the work, preliminary tests have been carried out by reacting cyclohexanone in the presence of two different bio-oil samples at 10 wt% each. Compared to literature [15–17], which showed > 96 % cyclohexanone yields from lignin-derived bio-oils, the choice of 10 wt% bio-oil addition should provide measurable effects of these bio-oils on C-C coupling of cyclohexanone in these preliminary tests. The reactions were studied under hydrogen atmosphere and the same experimental conditions used for pure cyclohexanone. The compositions of the mixed feedstocks (9:1 mass ratios of cyclohexanone to each bio-oil) were determined by GC–MS (Supplementary Information Tables S7 and S8).

Table 7
Effect of bio-oil on cyclohexanone product yields, conversion and selectivity of C-C coupling products at 160 °C, 9 g cyclohexanone, 1 g bio-oil, 0.5 g $NbOPO_4$ catalyst loading, and 10 bar initial hydrogen pressure.

Product yields (Two Pot – 1st Stage), 160 °C (3 h)	CYC	CYC + 10 wt % Bio-oil A	CYC + 10 wt % Bio-oil B
Liquid (wt%)	93.6 ± 1.80	99.4 ± 1.63	98.2 ± 1.38
Gas (wt%)	3.39 ± 0.21	0.04 ± 0.19	0.1 ± 0.32
Solid (wt%)	0.64 ± 0.16	0.35 ± 0.13	0.4 ± 0.17
Product yields (Two Pot – 2nd Stage), 300 °C (3 h)	CYC	CYC + 10 wt % Bio-oil A	CYC + 10 wt % Bio-oil B
Liquid (wt%)	86.3 ± 1.45	87.7 ± 1.22	90.5 ± 0.87
Gas (wt%)	8.51 ± 0.17	1.36 ± 0.30	0.84 ± 0.18
Solid (wt%)	0.62 ± 0.11	5.25 ± 0.41	5.48 ± 0.23
Product yields (One Pot – 2 Stages), 160 °C (3 h), then 300 °C (3 h)	CYC	CYC + 10 wt % Bio-oil A	CYC + 10 wt % Bio-oil B
Liquid (wt%)	87.8 ± 0.96	90.6 ± 1.27	93.7 ± 0.82
Gas (wt%)	6.18 ± 0.43	1.45 ± 0.14	0.50 ± 0.28
Solid (wt%)	1.59 ± 0.18	4.60 ± 1.04	3.20 ± 0.83
Conversion and liquid compositions (Two Pot – 1st Stage), 160 °C (3 h)	CYC	CYC + 10 wt % Bio-oil A	CYC + 10 wt % Bio-oil B
Cyclohexanone conversion (%)	68.4 ± 2.21	32.0 ± 1.73	15.0 ± 1.44
Sel. (%) of No C-C oxygenated condensates	0.0 ± 0.0	0.0 ± 0.0	6.71 ± 0.85
Sel. (%) of Single C-C oxygenated condensates	59.2 ± 2.63	62.2 ± 2.37	92.5 ± 1.93
Sel. (%) of 2 + C-C oxygenated condensates	28.3 ± 2.81	0.9 ± 0.27	nd
Sel. (%) of Hydrocarbons	11.9 ± 1.06	nd	0.6 ± 0.04

CYC = Cyclohexanone; Sel. = Selectivity; nd = not detected.

Table 7 shows the results of the aldol condensation (first) stage at 160 °C in the presence of the two bio-oil samples using $NbOPO_4$ (two pot – two stages) and 30 wt% Ni/$NbOPO_4$ (one pot – two stages). The results of cyclohexanone alone at this stage has been repeated in Table 7 for ease of comparison. The product yields showed that during the first stage of the two-pot system, the mixed liquid feedstocks remained largely unchanged, with the reaction producing very small amounts of solid and gas products, compared to when cyclohexanone was reacted alone. At 300 °C, for both systems, liquid products from the mixed feedstocks remained dominant (≥ 90 wt%) and somewhat similar to that of pure cyclohexanone. However, significant differences could be observed in the yields of gas and solid products with the mixed feedstocks compared to only cyclohexanone for both systems. With cyclohexanone alone, much more gas than solid residue was produced at all temperatures, whereas for the cyclohexanone/bio-oil mixtures, much more solid residues that gas products were obtained. Therefore, the presence of the bio-oil influenced increased formation of solid residue and suppressed gas formation.

From GC–MS analysis, it became clear that the presence of bio-oil significantly reduced the conversion of cyclohexanone during the first stage (160 °C, 3 h) from 68.4 % for pure cyclohexanone feedstock to 32 % for Bio-oil A and 15 % for Bio-oil B as shown in Table 7. This could be due to two reasons: (1) the organic compounds in the bio-oil and cyclohexanone competed for the $NbOPO_4$ catalyst's acid sites; (2) poor volatilisation effects caused by the presence of higher boiling point components in the bio-oils (e.g., phenol BP = 181.7 °C vs cyclohexanone BP = 155.6 °C), thereby, preventing the cyclohexanone vapour to reach the suspended catalyst bed.

The results of second stage two-pot reaction and one-pot sequential aldol condensation with 30 wt% Ni/$NbOPO_4$ are shown in Fig. 10. After reaction, the conversions of cyclohexanone for cyclohexanone/bio-oil feedstock were 98.4 % (two-pot and Bio-oil A), 85.3 % (two-pot and Bio-oil B), 94.3 % (one-pot and Bio-oil A), and 81.7 % (one-pot and Bio-oil B) compared with 99 % obtained for pure cyclohexanone with the same catalyst (Sections 3.2.2 and 3.3). Therefore, the presence of different bio-oil components in the mixed feedstocks reduced the conversion of cyclohexanone. Hence, possible competition for acid and metal sites could have led to a considerable decrease in selectivity towards naphthene, alkyl naphthene, alkyl aromatic, and partially hydrogenated polyaromatic for cyclohexanone/bio-oil feedstock. For two-pot sequential aldol condensation and HDO, the selectivity towards the different classes of hydrocarbons gave a similar pattern to conversion, particularly for naphthene, alkyl naphthene, and partially hydrogenated polyaromatic (Fig. 10a). However, in the one-pot system, the selectivity

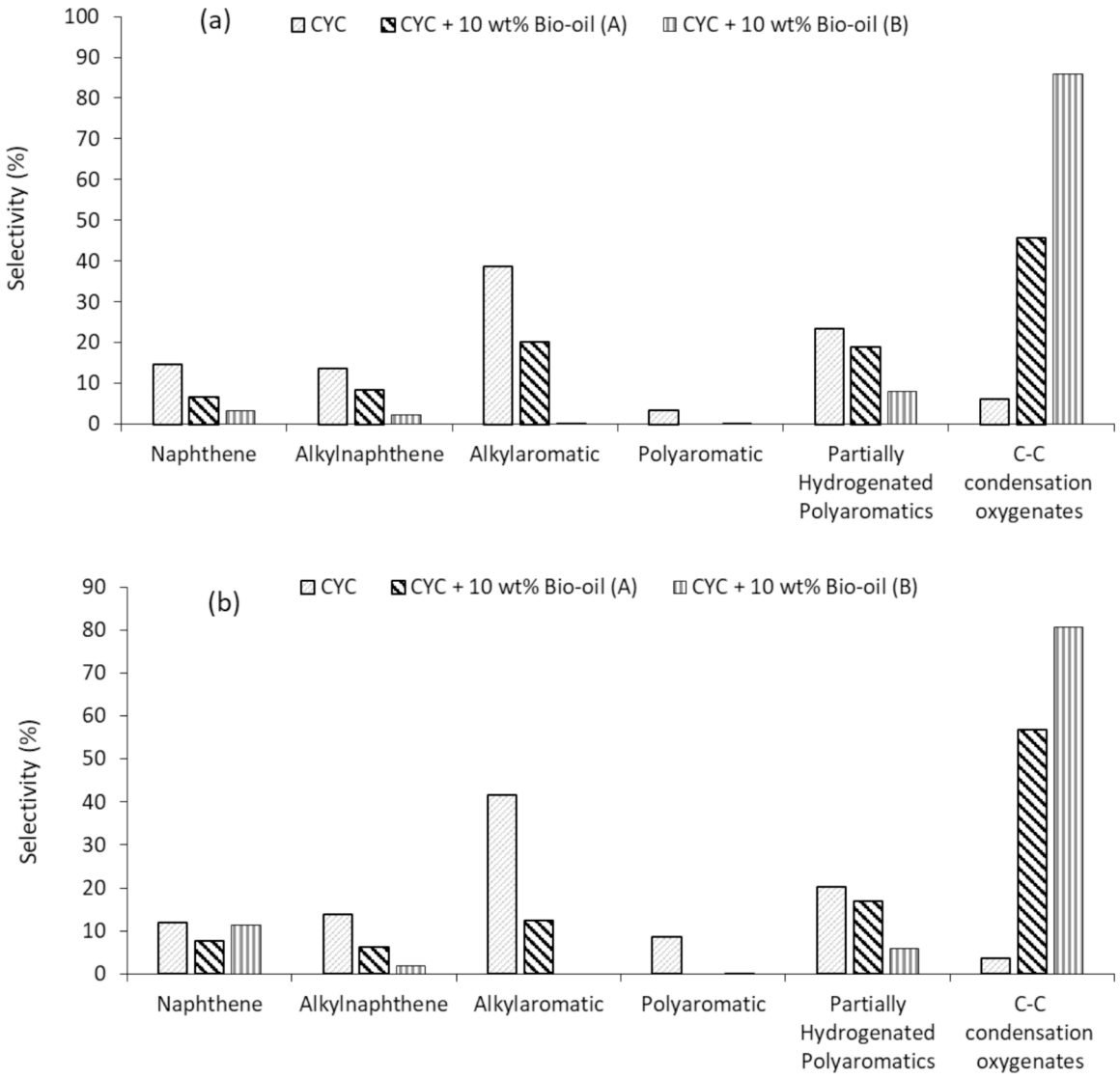

Fig. 10. Effect of 1 g bio-oil in 9 g cyclohexanone on the distribution of hydrocarbon products: (a) in two-pot second stage HDO reaction using 0.5 g 30 wt% Ni/$NbOPO_4$, 300 °C, initial hydrogen pressure 10 bar, and time of 3 h; (b) One-pot aldol condensation (160 °C for 3 h) followed by HDO (300 °C for 3 h) using 0.5 g 30 wt% Ni/$NbOPO_4$ catalyst at 10 bar initial hydrogen pressure [note: CYC = cyclohexanone].

for naphthene followed the trend of pure CYC > CYC + 10 wt% Bio-oil B > CYC + 10 wt% Bio-oil A, whereas the selectivity for alkyl naphthene and partially hydrogenated polyaromatic was similar with the pattern reported in the two-pot process (Fig. 10b). Thus, Bio-oil B produced a stronger effect on the conversion of cyclohexanone than Bio-oil A. Overall, the presence of bio-oil greatly inhibited the production of polyaromatic hydrocarbons during the aldol condensation and HDO stages when compared to cyclohexanone alone as the feedstock.

Interestingly, for the cyclohexanone/bio-oil feedstocks, single C-C adduct oxygenate products exhibited greater selectivity than for cyclohexanone alone, while the production of 2 + C-C oxygenated condensates and hydrocarbons were significantly decreased. In comparison to cyclohexanone alone as feedstock, the selectivity towards C-C adduct condensation oxygenate products was significantly higher with cyclohexanone/bio-oil feedstocks. Fig. 10 shows that most of the oxygenate products are C-C coupled adducts, demonstrating the ability of the 30 wt% Ni/$NbOPO_4$ to concurrently activate C-C coupling during second stage at 300 °C, even in the presence of bio-oil. However, the presence of the bio-oils and their components greatly suppressed the sequential deoxygenation and dehydration of C-C adducts to form hydrocarbons during second stage, compared to results with cyclohexanone alone. Therefore, future studies with cyclohexanone/bio-oil feedstocks should consider the optimisation of reaction temperature in the aldol condensation stage and the optimisations of reactor configuration, metal loading on the $NbOPO_4$ and/or hydrogen pressure during the second stage to achieve the required HDO level to produce hydrocarbons.

4. Conclusion

Aviation fuel range hydrocarbons can be synthesised using platform compounds produced from lignocellulosic biomass. This is viewed as an approach to incorporate low carbon alternatives and decarbonise the industry. Since the carbon length of these biomass-derived platform molecules are short (C_2-C_8), to increase the density and thermal stability of the potential aviation fuel would require a catalyst that can activate C-C coupling reactions. For carbon-chain elongation to be realised, aldol condensation and alkylation are basic C-C coupling processes.

In this present work, aviation fuel high density fractions such as mono-cycloalkanes, bi-cycloalkanes, and alkyl aromatics hydrocarbons have been produced through self-aldol condensation of cyclohexanone using $NbOPO_4$ catalyst followed by hydrodeoxygenation with 30 wt%

$Ni/NbOPO_4$, 5 wt% Pd/Al_2O_3, 30 wt% Ni/SiO_2, and 30 wt% Ni/ZrO_2-SiO_2 catalysts with two-pot reactors. Among the catalysts investigated, it was found that 30 wt% $Ni/NbOPO_4$ gave superior activity, achieving cyclohexanone conversion of about 99 % and hydrocarbons selectivity of 94 %, followed by 5 wt% Pd/Al_2O_3 98.4 % (conversion) and 72 % (hydrocarbons), and 30 wt% Ni/ZrO_2-SiO_2 exhibited poor hydrodeoxygenation activity. The superior catalytic activity of $NbOPO_4$ is related to its high number of surface sites maintaining acid characteristics and higher specific surface area. The results show that more alkylated cycloalkanes and aromatic were produced when 30 wt% $Ni/NbOPO_4$ catalyst was used in the hydrodeoxygenation phase compared to 5 wt% Pd/Al_2O_3 catalyst. The hydrogenation functionality of Ni metal incorporated into $NbOPO_4$ converted polyaromatic hydrocarbons into partially hydrogenated polycyclic products. However, more coke, and gas (especially, CO and CO_2) yields were observed for 30 wt% $Ni/NbOPO_4$ than 5 wt% Pd/Al_2O_3 catalyst, possibly due to the stronger acid sites of the $NbOPO_4$ than Al_2O_3. The 30 wt% $Ni/NbOPO_4$ catalyst produced similar results, in terms of liquid yields and compositions, in a one-pot two-step system, albeit, with slightly higher coke formation. When reacted with 10 wt% bio-oil, the conversion of cyclohexanone via aldol C-C coupling at 160 °C was significantly reduced, but this improved and became highly selective for single C-C coupling oxygenates at 300 °C. In addition, the bio-oils inhibited the formation of hydrocarbons compared to pure cyclohexanone at 300 °C, by preventing deoxygenation and dehydration reactions of the C-C coupled oxygenates. Consequently, these results showed that the optimisation of reaction temperature during the aldol condensation stage should be given sufficient consideration in future study involving cyclohexanone/bio-oil feedstock. This work has shown the feasibility of producing high-density aviation fuel component hydrocarbons from biomass-derived cyclohexanone by integrating aldol condensation and hydrogenation. However, the novel $NbOPO_4$-supported Ni catalyst requires fine tuning of the surface characteristics to minimise the formation of polyaromatic hydrocarbons but instead enhance the selectivity towards aviation fuel range naphthenes and alkylated aliphatic hydrocarbons.

CRediT authorship contribution statement

Abarasi Hart: Writing – original draft, Visualization, Validation, Methodology, Investigation, Formal analysis, Data curation. **Jude A. Onwudili:** Writing – review & editing, Writing – original draft, Visualization, Supervision, Resources, Project administration, Methodology, Funding acquisition, Conceptualization. **Eyup Yildirir:** Visualization, Methodology, Investigation, Data curation. **Seyed E. Hashemnezhad:** Data curation, Formal analysis, Investigation, Methodology, Writing – review & editing.

Funding

This work was supported by Innovate UK Energy Catalyst Round 8: Clean Energy – Experimental Development (Project Number 75521) and Innovate UK Energy Catalyst Round 9 – Mid Stage (Project Number 10047783).

Declaration of competing interest

The authors declare that they have no known competing financial interests or personal relationships that could have appeared to influence the work reported in this paper.

Acknowledgements

The authors would like to thank the Innovate UK for funding this work. In addition, the authors are grateful to the Energy & Bioproducts Research Institute (EBRI) and Aston University, UK for all the support received.

Appendix A. Supplementary data

Supplementary data to this article can be found online at https://doi.org/10.1016/j.cej.2025.161494.

Data availability

Data will be made available on request.

References

[1] J. Xu, et al., Synthesis of high-density aviation fuels with methyl benzaldehyde and cyclohexanone, *Green Chem.* 20 (16) (2018) 3753–3760, https://doi.org/10.1039/c8gc01628c.
[2] J. Holladay, Z. Abdullah, J. Heyne, "Sustainable Aviation Fuel: Review of Technical Pathways Report," Sep. 2020.
[3] N. Li, G.W. Huber, Aqueous-phase hydrodeoxygenation of sorbitol with Pt/SiO_2-Al_2O_3: identification of reaction intermediates, *J. Catal.* 270 (1) (2010) 48–59, https://doi.org/10.1016/j.jcat.2009.12.006.
[4] W. Wang, et al., Synthesis of renewable high-density fuel with cyclopentanone derived from hemicellulose, *ACS Sustain. Chem. Eng.* 5 (2) (2017) 1812–1817, https://doi.org/10.1021/acssuschemeng.6b02554.
[5] J.A. Onwudili, V. Sharma, C.A. Scaldaferri, A.K. Hossain, Production of upgraded fuel blend from fast pyrolysis bio-oil and organic solvent using a novel three-stage catalytic process and its combustion characteristics in a diesel engine, *Fuel* 335 (November 2022) (2023) 127028, https://doi.org/10.1016/j.fuel.2022.127028.
[6] G.W. Huber, S. Iborra, A. Corma, Synthesis of transportation fuels from biomass: chemistry, catalysts, and engineering, Chem. Rev. 106 (9) (2006) 4044–4098, https://doi.org/10.1021/cr068360d.
[7] J. Donnelly, R. Horton, K. Gopalan, C.D. Bannister, C.J. Chuck, Branched ketone biofuels as blending agents for Jet-A1 aviation kerosene, *Energy Fuel* 30 (1) (2016) 294–301, https://doi.org/10.1021/acs.energyfuels.5b01629.
[8] E.R. Sacia, M. Balakrishnan, M.H. Deaner, K.A. Goulas, F.D. Toste, A.T. Bell, Highly selective condensation of biomass-derived methyl ketones as a source of aviation fuel, *ChemSusChem* 8 (10) (2015) 1726–1736, https://doi.org/10.1002/cssc.201500002.
[9] F. Han, et al., Synthesis of renewable aviation fuel additives with aromatic aldehydes and methyl isobutyl ketone under solvent-free conditions, *Sustain. Energy Fuels* 5 (2) (2021) 556–563, https://doi.org/10.1039/d0se01544j.
[10] Z. Li, S. Shao, X. Hu, X. Li, Y. Cai, Insight into the production of aviation fuel by aldol condensation of biomass-derived aldehydes and ketones followed by hydrogenation, *Biomass Convers. Biorefin.* 14 (6) (2024) 7915–7926, https://doi.org/10.1007/s13399-022-03083-y.
[11] X. Li, J. Sun, S. Shao, X. Hu, Y. Cai, Aldol condensation/hydrogenation for jet fuel from biomass-derived ketone platform compound in one pot, *Fuel Process. Technol.* 215 (2021), https://doi.org/10.1016/j.fuproc.2021.106768.
[12] P. Li, et al., Bio-oil from biomass fast pyrolysis: yields, related properties and energy consumption analysis of the pyrolysis system, *J. Clean. Prod.* 328 (2021) 129613, https://doi.org/10.1016/j.jclepro.2021.129613.
[13] L. Faba, E. Díaz, S. Ordóçez, One-pot aldol condensation and hydrodeoxygenation of biomass-derived carbonyl compounds for biodiesel synthesis, *ChemSusChem* 7 (2014) 2816–2820, https://doi.org/10.1002/cssc.201402236.
[14] S. Shao, et al., Integrated C–C coupling/hydrogenation of ketones derived from biomass pyrolysis for aviation fuel over Ni/Mg–Al–O/AC bifunctional catalysts, *J. Clean. Prod.* 282 (2021) 124331, https://doi.org/10.1016/j.jclepro.2020.124331.
[15] A. Bakhtyari, A. Sakhayi, M.R. Rahimpour, S. Raeissi, Upgrading of cyclohexanone to hydrocarbons by hydrodeoxygenation over nickel–molybdenum catalysts, *Int. J. Hydrogen Energy* 45 (19) (2020) 11062–11076, https://doi.org/10.1016/j.ijhydene.2020.02.036.
[16] Q. Meng, M. Hou, H. Liu, J. Song, B. Han, Synthesis of ketones from biomass-derived feedstock, *Nat. Commun.* 8 (2017) 14190, https://doi.org/10.1038/ncomms14190.
[17] H. Liu, T. Jiang, B. Han, S. Liang, Y. Zhou, Selective phenol hydrogenation to cyclohexanone over a dual supported Pd–Lewis acid catalyst, *Science* 326 (5957) (1979) 1250–1252, https://doi.org/10.1126/science:1178606.
[18] A. Bakhtyari, A. Sakhayi, Z. Moravvej, R.M. Rahimpour, Converting cyclohexanone to liquid fuel – grade products: a characterization and comparison study of hydrotreating molybdenum catalysts, *Catal Letters* 151 (11) (2021) 3343–3360, https://doi.org/10.1007/s10562-021-03575-y.
[19] P. Carniti, A. Gervasini, F. Bossola, V. Dal Santo, Cooperative action of Brønsted and Lewis acid sites of niobium phosphate catalysts for cellobiose conversion in water, *Appl. Catal. B* 193 (2016) 93–102, https://doi.org/10.1016/j.apcatb.2016.04.012.
[20] K. Nakajima, et al., $Nb_2O_5 \bullet nH_2O$ as a heterogeneous catalyst with water-tolerant lewis acid sites, *J. Am. Chem. Soc.* 133 (12) (2011) 4224–4227, https://doi.org/10.1021/ja110482r.
[21] X. Wang, Y. Song, C. Huang, B. Wang, Crystalline niobium phosphates with water-tolerant and adjustable Lewis acid sites for the production of lactic acid from triose sugars, *Sustain. Energy Fuels* 2 (7) (2018) 1530–1541, https://doi.org/10.1039/c8se00140e.
[22] Q. Xia, Y. Wang, "Niobium-Based Catalysts for Biomass Conversion," in *Nanoporous Catalysts for Biomass Conversion*, First., C. V. Stevens, F.-S. Xiao, and L. Wang, Eds.,

John Wiley & Sons Ltd, 2017, pp. 253–275. doi: https://doi.org/10.1002/9781119128113.ch11.
[23] Y. Zhang, et al., Mesoporous niobium phosphate : an excellent solid acid for the dehydration of fructose to 5-hydroxymethylfurfural in water, *Cat. Sci. Technol.* 2 (2012) 2485–2491, https://doi.org/10.1039/c2cy20204b.
[24] Y. Wang, J. Ma, D. Liang, M. Zhou, F. Li, R. Li, Lewis and Brønsted acids in super-acid catalyst SO_4^{2-}/ZrO_2-SiO_2, *J. Mater. Sci.* 44 (24) (2009) 6736–6740, https://doi.org/10.1007/s10853-009-3603-8.
[25] T. Barzetti, E. Selli, D. Moscotti, L. Forni, Pyridine and ammonia as probes for FTIR analysis of solid acid catalysts, *J. Chem. Soc. Faraday Trans.* 92 (8) (1996) 1401–1407.
[26] T. Li, et al., The synergistic effect of Cu0 and Cu+ for one-step synthesis of aviation biofuel from biomass-derived ketones, *Green Chem.* 26 (4) (2024) 1910–1926, https://doi.org/10.1039/d3gc02671j.
[27] E. Rodríguez-Castellón, et al., Nickel-impregnated zirconium-doped mesoporous molecular sieves as catalysts for the hydrogenation and ring-opening of tetralin, *Appl. Catal. A Gen.* 240 (2003) 83–94.
[28] Z. Wei, H. Qiao, H. Yang, C. Zhang, X. Yan, Characterization of NiO nanoparticles by anodic arc plasma method, *J. Alloys Compd.* 479 (1–2) (2009) 855–858, https://doi.org/10.1016/j.jallcom.2009.01.064.
[29] M. Niculescu, P. Budrugeac, "STRUCTURAL CHARACTERIZATION OF NICKEL OXIDE OBTAINED BY THERMAL DECOMPOSITION OF POLYNUCLEAR COORDINATION COMPOUND [Ni 2 (OH)2 (H3 CCH(OH)COO-)2(H2O)2·0.5H2O] n," *Rev. Roum. Chim*, vol. 58, no. 4–5, pp. 381–386, 2013, [Online]. Available: http://web.icf.ro/rrch/.
[30] N. Cardona-Martínez, J.A. Dumesic, Acid strength of silica-alumina and silica studied by microcalorimetric measurements of pyridine adsorption, *J. Catal.* 125 (1990) 427–444.
[31] H.J.M. Bosman, E.C. Kruissink, J. Vanderspoel, F. Vandenbrink, "Characterization of the acid strength of SiO_2-ZrO_2 mixed oxides," 148(2) 1994 660–672.
[32] A. Samikannu, et al., Highly dispersed NbOPO4/SBA-15 as a versatile acid catalyst upon production of renewable jet-fuel from bio-based furanics via hydroxyalkylation-alkylation (HAA) and hydrodeoxygenation (HDO) reactions, *Appl. Catal. B* 272 (2020), https://doi.org/10.1016/j.apcatb.2020.118987.
[33] Y. Zeng, et al., Cu/Mg/Al hydrotalcite-like hydroxide catalysts for o-phenylphenol synthesis, *Appl. Clay Sci.* 126 (2016) 207–214, https://doi.org/10.1016/j.clay.2016.03.017.
[34] A. Bakhtyari, A. Sakhayi, M.R. Rahimpour, S. Raeissi, The utilization of synthesis gas for the deoxygenation of cyclohexanone over alumina-supported catalysts: screening catalysts, *Asia Pac. J. Chem. Eng.* 15 (2) (2020) e2425, https://doi.org/10.1002/apj.2425.
[35] H. Tang, et al., Synthesis of jet fuel additive with cyclopentanone, *J. Energy Chem.* 29 (2019) 23–30, https://doi.org/10.1016/j.jechem.2018.01.017.
[36] N. Liang, X. Zhang, H. An, X. Zhao, Y. Wang, Direct synthesis of 2-ethylhexanol via n-butanal aldol condensation–hydrogenation reaction integration over a Ni/Ce-Al_2O_3 bifunctional catalyst, *Green Chem.* 17 (2015) 2959–2972, https://doi.org/10.1039/c5gc00223k.
[37] J.A. Onwudili, C.A. Scaldaferri, Catalytic upgrading of intermediate pyrolysis bio-oil to hydrocarbon-rich liquid biofuel via a novel two-stage solvent-assisted process, *Fuel* 352 (2023) 129015, https://doi.org/10.1016/j.fuel.2023.129015.
[38] S. Shao, X. Xia, X. Li, H. Zhang, R. Xiao, Aldol condensation of biomass-derived aldehydes and ketones followed by hydrogenation over Ni/HZSM-5 to produce aviation fuel: role of acid sites, *Fuel Process. Technol.* 250 (2023) 107904, https://doi.org/10.1016/j.fuproc.2023.107904.
[39] Y.S. Mahajan, R.S. Kamath, P.S. Kumbhar, S.M. Mahajani, Self-condensation of cyclohexanone over ion exchange resin catalysts : kinetics and selectivity aspects, *Ind. Eng. Chem. Res.* 47 (2008) 25–33.
[40] B.N. Barman, L. Skarlos, D.J. Kushner, Simultaneous determination of oil and coke contents in spent hydroprocessing catalyst by thermogravimetry, Energy Fuels (3) (1997) 593–595. Available: https://pubs.acs.org/sharingguidelines.
[41] J.B. Omajali, A. Hart, M. Walker, J. Wood, L.E. Macaskie, In-situ catalytic upgrading of heavy oil using dispersed bionanoparticles supported on gram-positive and gram-negative bacteria, *Appl. Catal. B* 203 (2017) 807–819, https://doi.org/10.1016/j.apcatb.2016.10.074.
[42] J. Li, X. Lv, Y. Wang, Q. Li, C. Hu, Hydrotreatment upgrading of bio-oil from torrefaction of pubescens in alcohol over Pd/$NbOPO_4$, *ACS Omega* 3 (5) (2018) 4836–4846, https://doi.org/10.1021/acsomega.8b00180.